Beams of radioactive nuclei

Yu. É. Penionzhkevich
Joint Institute for Nuclear Research, Dubna

Fiz. Elem. Chastits At. Yadra **25**, 930–1003 (July–August 1994)

The present status of experimental research in a new field of nuclear physics connected with the production and use of radioactive nuclear beams is described.

INTRODUCTION

Experimental investigations using beams of radioactive nuclei are a new intensively developing direction of heavy-ion physics that during the last 30 years has passed through several stages of development. When the first heavy-ion beams became available, nuclear physics acquired a powerful method for investigating fundamental properties of nuclear matter. In reactions involving the interaction of two complicated nuclei it became possible to obtain nuclei in an extreme state—strongly heated "madly" rotating nuclei with anomalously high ratio of the neutron–proton number and strongly deformed. This was why the commissioning at Dubna in 1960 of one of the first powerful heavy-ion accelerators—the U-300 cyclotron—permitted the scientific collaboration of the Laboratory of Nuclear Reactions, under the direction of Academician G. N. Flerov, to make numerous important discoveries that fostered the development of new ideas about nuclear properties.[1] A new type of radioactivity—delayed proton decay[2] was discovered, and its investigation development into an entire direction of nuclear physics and made it possible to predict[3] and then discover proton decay from the ground state, two-proton decay, and cluster radioactivity. In heavy-ion reactions spontaneously fissioning isomers were discovered,[4] and the interpretation of their properties made it possible to reconsider from a new viewpoint the nuclear potential energy and confirm the decisive role of shell effects in the decay properties of heavy nuclei, for the description of which Strutinsky[5] introduced the so-called shell corrections. This provided the basis for an entire cycle of experiments on heavy-ion beams that led to the discovery of new elements with $102 \leqslant Z \leqslant 110$ (Ref. 8). In the Laboratory of Nuclear Reactions at the JINR the phenomenon of delayed fission, which can also be explained by the influence of shell effects in nuclear decay, was discovered at the end of the sixties. Finally, numerous new effects associated with the mechanism of interaction of two complicated nuclei were discovered. These included deep inelastic nucleon transfers in nuclei,[6] sequential triple fission of heavy nuclei,[7] "cold" fusion,[8] the emission of charged particles with energies near the kinematic limit,[9] and more.

Investigations in these directions using heavy-ion beams are being extended as a result of the commissioning in many countries of new powerful heavy-ion accelerators of intermediate energies—the accelerator complex UNILAC-SIS-ESR at Darmstadt in Germany, the complex GANIL at Caen in France, the heavy-ion cyclotron complex RIKEN in Japan, the superconducting cyclotron in Michigan in the United States, the heavy-ion cyclotron complex at Lan-chou in China, the superconducting cyclotron at Catania in Italy, and the heavy-ion cyclotron complex at the Flerov Laboratory of Nuclear Reactions at the JINR in Dubna (Russian).

This new direction of accelerators makes it possible to obtain heavy-ion beams with unique properties—they are monochromatic and have high intensity with low angle acceptance. The possibility of producing in modern accelerators high-intensity beams of charged particles all the way from protons and helium to uranium ions has made it possible in recent years to start a new stage in the investigation of nuclei using beams of radioactive nuclei. These investigations are made in two directions—the production of beams of exotic nuclei and the study of their properties, and also the investigation of reactions with beams of radioactive nuclei. This new direction of nuclear physics has already made it possible to obtain a number of very interesting results relating to the properties of nuclei far from the β-stability region. In these experiments, beams of radioactive nuclei with intensity 10^2–10^7 s^{-1} have been used. Experiments to study the interaction of radioactive nuclei with the matter of a target have been made at this intensity. Measurements have been made of the absorption cross sections, the Coulomb dissipation, and the angular scattering of some radioactive nuclei,[10] and analysis of these data has yielded information about the nucleon radii of the nuclei. A "neutron halo" has been discovered in the ^{11}Li nucleus, and searches are being made for "neutron halos" in other neutron-rich nuclei (^{6}He,^{8}He,^{14}Be, etc.), and also "proton halos" in neutron-deficient nuclei (^{8}Be,^{19}Na, etc.). However, for investigations of more complicated reactions with radioactive beams (transfer reactions, fusion–fission, fragmentation), which have cross sections $\sigma < 10^{-26}$ cm^2, it is necessary to have a beam intensity $I \geqslant 10^7$ s^{-1} (see Fig. 1), and also a detecting system with high detection efficiency in a solid angle close to 4π.

Thus, the problem of using radioactive beams for physics investigations reduces mainly to three problems: the production of beams of radioactive nuclei of the necessary intensity, acceleration of the beams to the necessary energy, and the detection of the products of nuclear reactions involving the radioactive nuclei or their decay products.

1. PRODUCTION OF BEAMS OF RADIOACTIVE NUCLEI

Two main methods are used to generate radioactive nuclei in reactions with charged particles. The first method consists of using heavy-ion beams accelerated to an energy greater than 30 MeV/A with subsequent bombarding of a target with them. In this case there is fragmentation of the bombarding nuclei with the production of nuclei in a wide

 1063-7796/94/040394-34$10.00

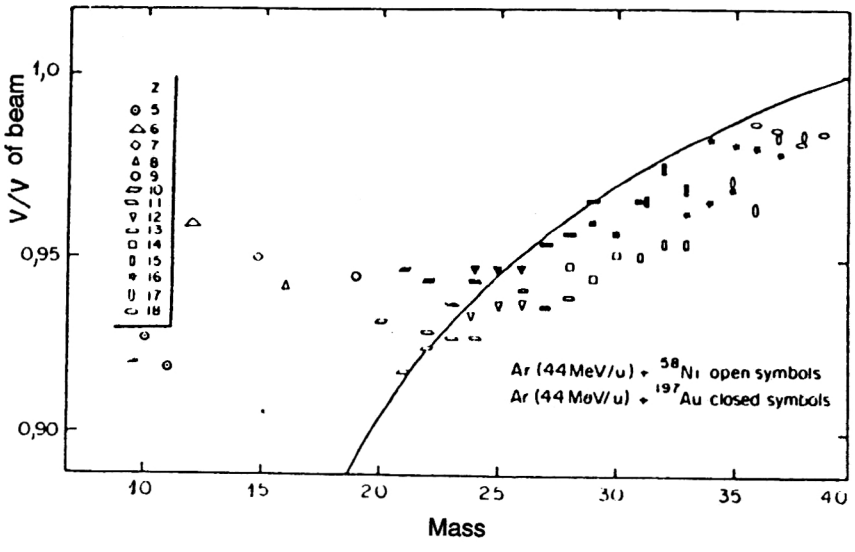

FIG. 1. Dependence of the ratio of the most probable velocity of the fragments to the beam velocity on the mass of the fragments.

range of charges and masses having a narrow forward-directed angular distribution and velocities comparable with the velocity of the primary beam. After the necessary nuclei have been separated in Z and A by means of magnetic fragment separators, one can use the obtained beams of radioactive nuclei without subsequent acceleration of them. The second method involves acceleration of protons or heavy ions to energies from 30 MeV/A to several GeV/A with subsequent bombarding of a thick target, which absorbs the entire energy of the bombarding particle. Then as a result of fragmentation (or spallation) of nuclei under the influence of the high-intensity beams, radioactive nuclei are obtained in a wide range of Z and A; these remain in the material of the target. For further use of these nuclei, they must be extracted from the target and accelerated to the necessary energy. This is achieved by using special ion sources and mass separators of the ISOL type in a facility with a system of ion transport of the gas-jet type and post acceleration.

The advantages of the first method is the possibility of obtaining beams of short-lived nuclei with lifetimes down to several hundred microsonds. However, because of the restriction on the target thickness ($\sim$500 mg$\cdot$cm^{-2}) the yield of radioactive nuclei is not so high as in the case of complete absorption of the ion in the target. To obtain relatively intense radioactive beams of nuclei with $\tau_{1/2} \geqslant 0.5$ s, the second method is, as a rule, used. The restriction on the lifetime of such nuclei is explained by the time of their diffusion from the target in special sources.

There was also recently proposed a project for obtaining beams of radioactive nuclei for which the source is the high-flow reactor at the Laue–Langevin Institute at Grenoble (PIAFE project).[11] Irradiating a ^{235}U target with a beam of thermal neutrons in the reactor core, it is possible to obtain a high yield of fragments with $A=80$–100. Transporting then the radioactive nuclei to a source of multicharged ions and accelerating them in the cyclotron, one can, given total efficiency $\sim 10^{-4}$ of the complete system, obtain beams of radioactive nuclei in the region of masses of the fission fragments with intensities up to 10^8 s^{-1}.

There has also recently been proposed a method for storing radioactive nuclei in storage rings with electron cooling, a heavy-ion accelerator with fragment separator being used as injector. Such systems have a luminosity of $\sim 10^{29}$ cm$^2\cdot$s^{-1}.

In view of the importance of the development of accelerator complexes capable of producing radioactive beams and in order to coordinate research at them, the NuPECC committee of the European Physical Society has set up a working group under R. H. Simpsen, and it has made recommendations for the further development of the physics and technology of radioactive beams in Europe. Therefore, in the following exposition I shall be guided also by these recommendations.[71]

The intensity of the secondary beams can be represented by the simple dependence

$$I_{\text{sec}} = I_{\text{trim}}(N_A/M)\sigma d\varepsilon_{\text{extr}}\varepsilon_{\text{transport}}\varepsilon_{\text{ionize}}\varepsilon_{\text{accel}} \tag{1}$$

where σ [cm^2] is the total cross section of the reaction, d[g/cm^3] is the thickness of the target, M is the mass number of the element of the target, N_A is Avogadro's number, and ε is the efficiency of the corresponding processes from the extraction of the nuclei from the target ($\varepsilon_{\text{extr}}$) to the extraction from the postaccelerator ($\varepsilon_{\text{accel}}$). Therefore, considering the various methods of producing radioactive beams, we must analyze all these factors, which must lead to maximum intensity of the beam.

1.1. The method of fragmentation of heavy ions

The products of the fragmentation reaction that emerge from the target, which is placed at the focus of the first separating dipole magnet, spread out in the focal plane of this magnet, where one can then, by means of a slit, separate definite products in accordance with their magnetic rigidity:

$$B\rho = k\frac{A}{q}\left[v\left(1+\frac{v}{2m_u}\right)\right]^{1/2}, \tag{2}$$

where $B[T]$ is the magnetic field of the spectrometer, $\rho[m]$ is the radius of curvature of the trajectory in the dipole mo-

ment, q is the ion charge of the product, m_u is the atomic mass unit (931.5 MeV), $k=(2m_u/c)^{1/2}=0.1438$, and v is the velocity of the fragments.

The second part of the spectrometer compensates the dispersion in its first part and focuses the achromatic beam in the focal plane of the spectrometer. As a rule, good optical properties of the beam are ensured by a system of quadrupoles and one or several sextupoles, which constitute a doubly achromatic system. It is clear from the expression (2) that fragments having the same velocity v are separated in accordance with their A/q ratio. At high energies, when the fragments are completely stripped and $q=Z$, the separation takes place in accordance with the A/Z ratio of the secondary beam.

The basis of this method is the fragmentation of the bombarding particle when it interacts with the target and the subsequent separation and transporting of the fragmentation products separated in accordance with Z and A.

In this connection, a very important parameter in estimating the efficiency of the separating systems is the distribution of the fragments with respect to the velocities and angles. On the fragmentation of a particle, the most probable velocities of the produced fragments correspond to the velocity of the particle. Beginning with values of the mass and velocity corresponding to the bombarding particle, the velocity decreases with decreasing mass by 90–95%, and then remains constant (Fig. 1). Such a dependence is determined by the binding energy of the individual nuclides that are emitted on fragmentation; this energy is ~8 MeV. The ratio of the velocities of an emitted particle with mass A and the bombarding particle can be represented by the semiempirical expression

$$v_A/v_P=[(E_PA-(A_P-A/8(E_PA_P))]^{1/2}(A_P/A)^{1/2}, \quad (3)$$

where A_p and v_p are the mass and velocity of the particle, and E_p is its energy per nucleon. The distribution of the velocities is Gaussian:[12]

$$\frac{d^2\sigma}{dE_f d\Omega}\alpha(A_fE_f)^{1/2}\exp\left\{-A_f\left(\frac{E_f\sin^2\Theta}{\sigma_\perp^2}+\frac{E_f\cos^2\Theta-2(E_f\langle E_f\rangle)^{1/2}\cos\Theta+\langle E_f\rangle}{\sigma_\parallel^2}\right)\right\}, \quad (4)$$

where $\sigma_\perp^2$ and $\sigma_\parallel^2$ are the width parameters of the parallel and perpendicular distributions of the fragment velocities, θ is the detection angle in the laboratory system, $\langle E_f\rangle$ is the most probable fragment energy, and $\alpha\langle A_fE_f\rangle$ is a parameter that determines the straggling of the particle and fragment as they pass through the target:

$$\alpha(A_f,E_f)_{1/2}=\sqrt{\langle\alpha_{1/2\text{strag}},p^2\rangle+\langle\alpha_{1/2\text{strag}},f^2\rangle}.$$

The distribution of the different fragments with respect to velocity is shown in Fig. 2.

Also shown are the results of calculation of the distribution in accordance with the expression (4), from which it can be seen that there is good agreement with the experiment except for the low-energy part, where obviously other reactions, for example, transfer reactions contribute. However, this does not prevent us from calculating with relatively high

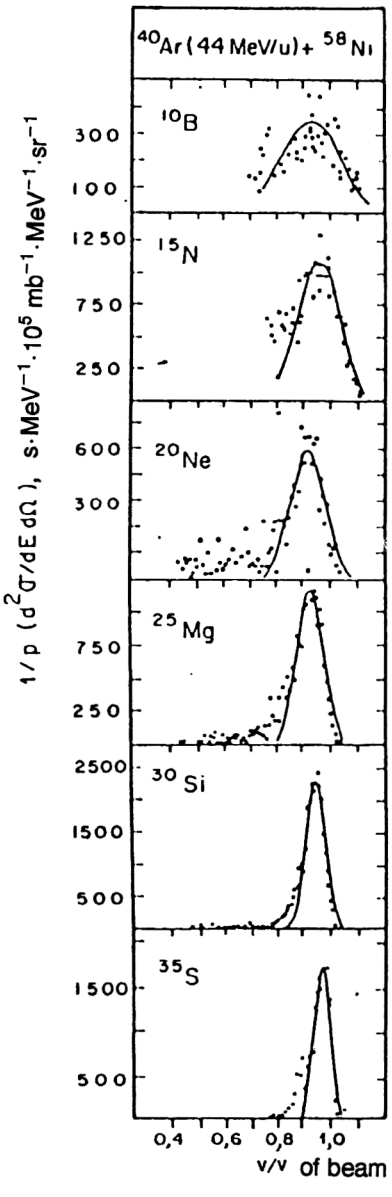

FIG. 2. Dependence of invariant reaction cross section measured at angle 3° on the ratio of the fragment velocity to the beam velocity.

accuracy the velocity distributions and, accordingly, the transmission of the fragments through the magnetic system.

The efficiency of the fragment separators is largely determined by their total solid angle and, for a fixed value of this, by the angular distribution of the fragments. At the present time, the angular distribution of the fragments is calculated using Goldhaber's model,[13] in which the perpendicular distribution of the angular momentum transfers is taken into account. Figure 3 shows typical angular distributions for various nuclei and curves calculated in accordance with the fragmentation model. It can be seen that at angles $\theta\geqslant5°$ the experimental cross sections lie above the calculated ones. In Ref. 14, this is explained by the contribution of the transfer reactions. As a rule, the maximum of the angular distribution is in the region of the grazing angle. This is clearly illustrated by the experimental data shown in Fig. 4. As follows from the experimental data, the main contribution to the cross sec-

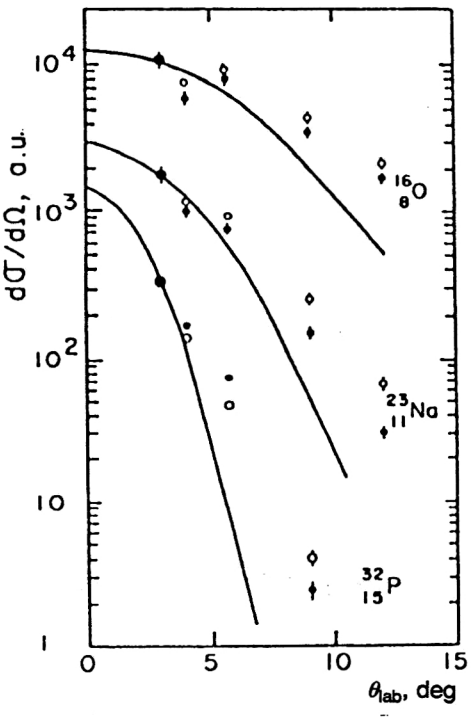

FIG. 3. Angular distribution of fragments in the reactions Ar+Ni (open symbols) and Ar+Au (closed symbols).

tion is made by products emitted at angle $\theta \leqslant 5°$. In addition, the angular distributions of the fragments depend strongly on their velocity (see Fig. 5). As yet, an exact description of the fragment angular distributions does not exist. The choice of the fragment separator acceptance is mainly based on experimental data.

The products obtained in this manner as a result of the fragmentation reaction have a broad distribution with respect to the mass and charge. To obtain a beam of radioactive nuclei with given Z and A, different methods of selecting the products are used. We consider these methods for the example of the now classical fragment separator LISE, which is operated at the GANIL National Center (Caen, France).[15] The scheme is shown in Fig. 6.

The spectrometer uses three methods of product selection: 1) magnetic selection in the first dipole; 2) selection using the difference of the energy losses in a special absorber in conjunction with a second dipole; 3) electrostatic selection using a Wien velocity selector.

The products of the fragmentation of the bombarding particle are analyzed in the magnetic field of the first dipole, which has magnetic rigidity $B\rho$, the choice being based on the condition that the required products should pass through the intermediate slit $F1$. The velocity and mass of the products are determined by the condition of equilibrium of the centrifugal and magnetic forces:

$$\frac{mv^2}{\rho}=QvB.$$

In the relativistic case, this equation takes the form

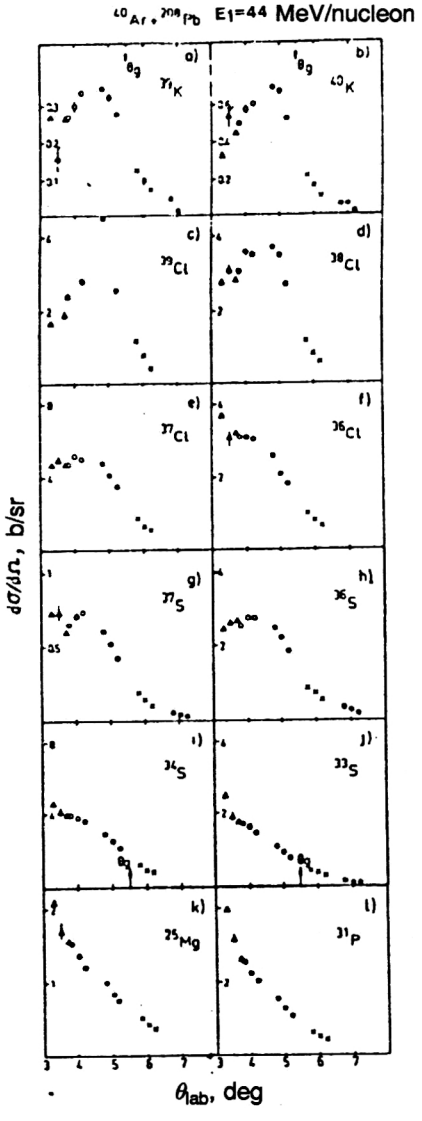

FIG. 4. Angular distribution of fragments closest in mass to the bombarding particle emitted in the reaction $^{208}Pb+^{40}Ar$ (44 MeV/nucleon).[12]

$$(B\rho)_f=\left(\frac{3.105\cdot AB\gamma}{Q}\right)_f, \quad \begin{cases}\gamma_f=\dfrac{E_f}{931.5}+1,\\ \beta_f=\sqrt{1-1/\gamma_f^2}\end{cases} \tag{5}$$

where ρ is the radius of curvature of the magnet. For the spectrometer LISE $\rho=2.003$ m. The mean energy of fragments produced from a bombarding particle of energy E_p1 is found by calculating the energy loss in a target of thickness d:

$$E_f=E_p1-1/2(\Delta E_p(E_p1,d/2)+\Delta E_f(E_p1-\Delta E_p(E_p1,d/2),d/2)). \tag{6}$$

The value of $\Delta E(x,y)$ is determined by the energy loss of a nucleus with initial energy x in a target of thickness y. The choice of the optimum rigidity $B\rho$ of the magnetic field is determined by the mean energy E_f.

The choice of the necessary target thickness is made by optimizing two opposite conditions—maximum yield of the products and maximum transmission of them through a spec-

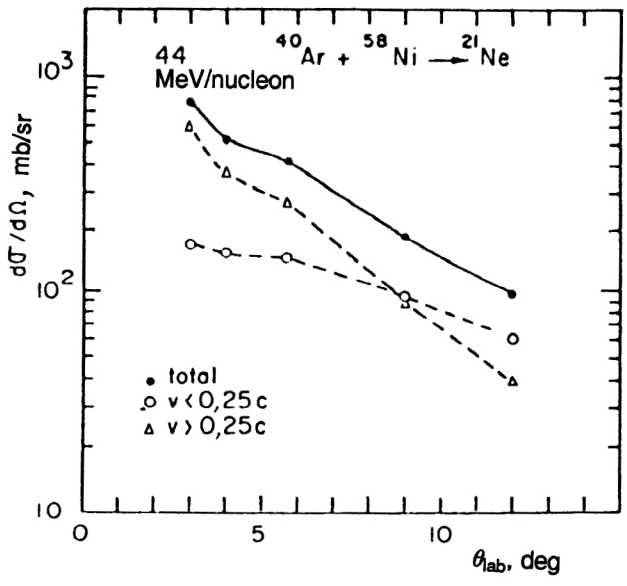

FIG. 5. Dependence of angular distributions of fragments on their velocity.

trometer that has a limited acceptance. The change in the energy due to the loss in the target relative to the chosen fragment energy $E_{f\ \text{chosen}}$ is determined by the ratio $\Delta E/E_{f\ \text{chosen}} = 2\Delta P/P_{f\ \text{chosen}} = 2\Delta B/B_{f\ \text{chosen}}$. Thus, for the spectrometer LISE, for which the slit size is $F1 = \pm 45$ mm and the dispersion in the first magnet is $D = 17.1$ mm%, the maximum spread of the fragment transmissions is $\Delta P/P = \pm 2.63\%$. The dispersion with respect to the product energy (straggling) is largely determined by the target thickness and also influences the coefficient of transmission of fragments through the first dipole.

The second dipole analyzes the fragments dispersed by the first magnet at the point $F2$ (see Fig. 7). The considered spectrometer is a double achromator with respect to the angle and position, and therefore the position of the beam at the point $PF2$ of the focal image does not depend on the angle and position of the entrance beam. In spectrometers of such type, one uses time-of-flight measurement of the particle trajectory, since all the particles traverse the same distance.

For additional filtering of the reaction products, a special absorber is also introduced between the two dipoles. Then the second dipole ($B\rho_2$) will analyze products as a function of their energy loss in the absorber:

$$(B\rho_2)_f = \left(\frac{3.105 \cdot A\beta_2\gamma_2}{Q}\right)_f, \tag{7}$$

where $E_f2 = E_f1 - \Delta E(E_f1, \langle d_{\text{abs}}\rangle)$, where $\langle d_{\text{abs}}\rangle$ is the mean thickness of the absorber.

In order to preserve the achromatization, the absorber must have a shape that satisfies the following condition: The ratio of the energies of two identical fragments (with the same A and Z) must be the same before and after the absorber:

$$\frac{E_f2}{E_f1} = \frac{E'_f2}{E'_f1} = \delta. \tag{8}$$

Knowing the dispersion D of the spectrometer, we can determine the position (P_f) of the fragments:

$$(P_f2) = P_f1\left(1 + \frac{x}{D}\right),$$

and hence

$$\frac{(P_f1)^2}{(P_f2)^2} = (1 + x/D)^2 = \frac{E_f2}{E_f1} = \delta; \tag{9}$$

using the Bethe approximation for the energy loss ($dE/dx \sim AZ^2/E$), we can write

$$E'_f1 - E_f1 = (dE/dx)_{\text{abs}} \sim \frac{AZ^2 d_{\text{abs}}}{E_f1}, \tag{10}$$

and also

$$E'_f2 - E_f2 = (dE/dx)_{\text{abs}} \sim \frac{AZ^2 d'_{\text{abs}}}{E_f2} = \frac{Z^2 d'_{\text{abs}}}{(\delta E_f1)}, \tag{11}$$

and bearing in mind that $E'_f2 - E_f2 = \delta(E'_f1 - E_f1)$, we obtain

$$\frac{(E'_f2 - E_f2)}{(E'_f1 - E_f1)} = \delta = \frac{AZ^2 d'_{\text{abs}} E_f1}{\delta AZ^2 d_{\text{abs}} E_f1} \tag{12}$$

$$\delta^2 = \frac{d'_{\text{abs}}}{d_{\text{abs}}} = (1 + x/D)^4. \tag{13}$$

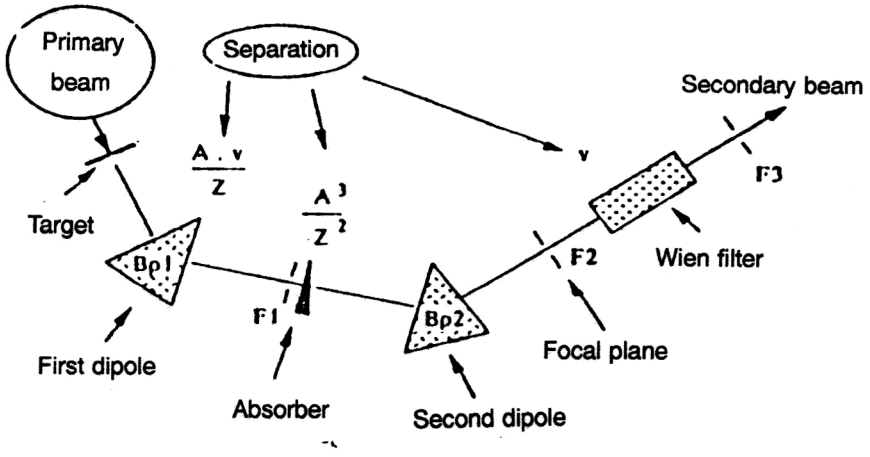

FIG. 6. Schematic arrangement of fragment separator with three methods of separation (magnetic, by energy loss, and electrostatic).

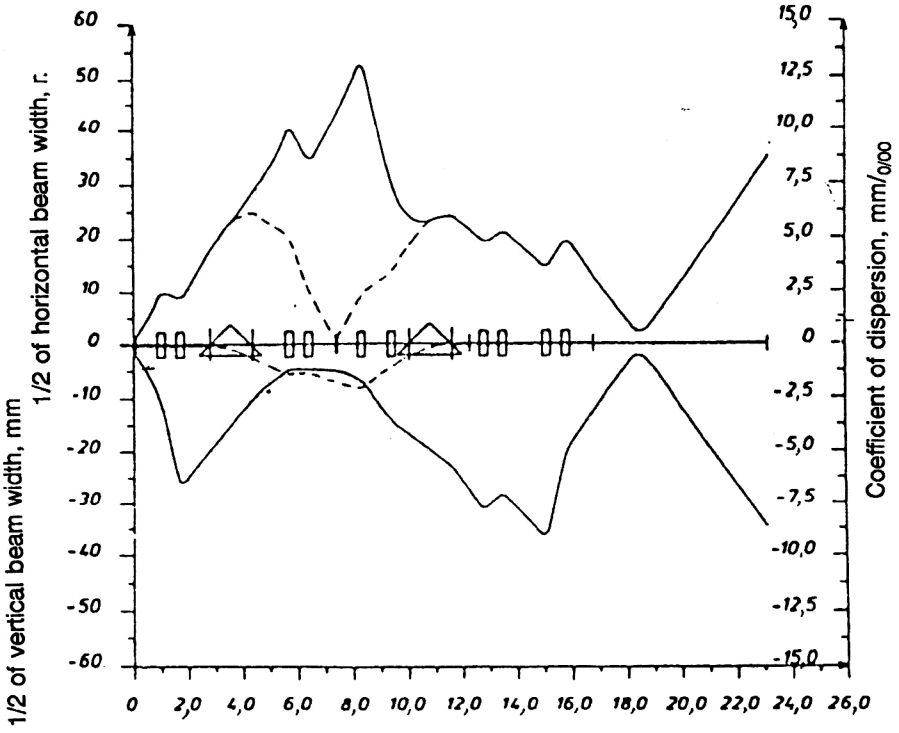

FIG. 7. Dispersion of beam in the horizontal and vertical planes of the fragment separator. The numbers along the abscissa are given in meters.

Thus, the thickness of the absorber, which changes with respect to the horizontal position x, is described by the expression given above. The absorber, ensuring different energy losses for the same fragments $(A_f Z_f)$, makes possible efficient selection of them. One can show fairly easily that the value of the energy at the exit of the first dipole, determined by the expression $B\rho \sim A_f v_f / Z_f$, gives for the velocity $v_f \approx Z_f/A_f$ or, for the energy, $E_f \approx Z_f^2/A_f$. These fragments lose in the absorber the energy

$$\frac{dE_f}{dx} \sim \frac{A_f Z_f^2}{E_f} \quad \text{or} \quad \frac{dE_f}{E_f} \sim \frac{A_f Z_f^2 d_{\text{abs}}}{E_f^2} \sim \frac{A^3 d_{\text{abs}}}{Z^2}.$$

We find that the relative energy loss by the fragments is given by[15]

$$\frac{dE}{dx} \sim \frac{A^3 d_{\text{abs}}}{Z^2}, \tag{14}$$

and a change of the magnetic field $dB/B = 1/2 dE/E$ makes it possible to choose nuclei with one value of A^3/Z^2. Figure 8 illustrates the possibility of using an absorber between the two dipoles to choose a definite region of nuclei and, accordingly, make an additional filtering out of the other reaction products.

Finally, for additional filtering out of beam fragments an electrostatic Wien filter is used after the second dipole. The electrostatic filter has an electric field and an increasing magnetic field, which acts on (A,Z) nuclei with corresponding force $F_e = QE$ and $F_m = QvB$.

In the case of equality of these forces, nuclei with veloc-

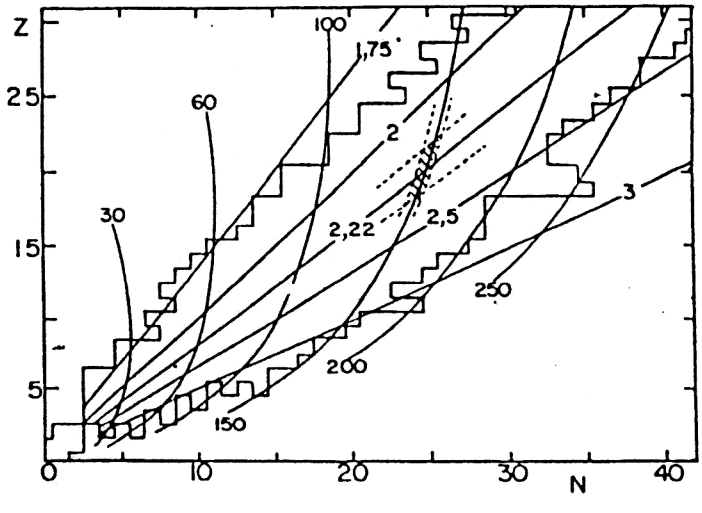

FIG. 8. Schematic representation of the effect of isotope separation by dipoles for different values of $B\rho$ (straight lines) and by absorbers of different thicknesses (the A^3/Z^2 curves) in the N, Z plane.

TABLE Ia. Accelerator facilities using fragmentation of heavy ions to produce radioactive beams.

Facility	Accelerator for initial beam	A	E, MeV/A	I, s^{-1}	Status of facility
B1/B42/B44 ion channel at LBL, Berkeley, USA	Bevalac, 8–2100 MeV/A, $\leqslant 10^9$ particles/s	$\leqslant 50$	$\leqslant 800$	$\leqslant 10^8$	Operating
LISE-3, GANIL, Caen, France	Tandem of two K-320 cyclotrons, 25–100 MeV/A, $\leqslant 10^{12}$ particles/s	$\leqslant 136$	$\leqslant 80$	$\leqslant 10^9$	Operating; it is proposed to raise the initial intensity and increase the efficiency of the fragment separator
RIPS, RIKEN, Vako, Japan	Cyclotron K-540, 30–135 MeV/A, $\leqslant 10^{11}$ particles/s	$\leqslant 136$	$\leqslant 110$	$\leqslant 10^8$	Operating
A1200, MSU, East Lansing, USA	Superconducting cyclotron, K-1200, 30–180 MeV/A, $\leqslant 100^{11}$ particles/s	30–180 MeV/A, $\leqslant 10^{11}$ particles/s	$\leqslant 136$	$\leqslant 150$	$\leqslant 10^8$
FRS/ESR GSI, Darmstadt, German Federal Republic	Synchrotron SIS18, 10–200 MeV/A, $\leqslant 10^8$ particles/s $\leqslant 10^{11}$ particles/s	$\leqslant 238$	$\leqslant 1000$	$\leqslant 10^5$ ($\leqslant 10^8$)	Operating; it is planned to increase the intensity in 1995
Heavy-ion accelerator facility, fragment separator KOMBAS, JINR, Dubna, Russia	Tandem of cyclotrons U-400–U-400M, 10–100 MeV/A, $\leqslant 10^{12}$ particles/s	$\leqslant 136$	$\leqslant 80$	$\leqslant 10^9$	Will be completed in 1995–1996

ity $v_0=E/B$ are not deflected and enter the slit ($F3$) at the filter exit. The size of the image of the fragment beam at the filter exit is given by

$$\sigma_x=\sqrt{F_0^2(\Delta v/v_0)^2 D_{\text{filter}}^2}, \tag{15}$$

where F_0 measures the size of the beam image on the target and D_{filter} is the dispersion of the velocities, determined by the semiempirical expression

$$D_{\text{filter}}=\frac{9.1\cdot 10^{-4} V l_E^2}{B\rho\beta_0}, \tag{16}$$

where V is the potential of the filter in kilovolts for fragments with $\beta\approx 0.3$, and 1_E is the length of the filter in meters. For the spectrometer LISE $D_{\text{filter}}=2$ mm/%. This means that two nuclei with $\Delta v/v=5\%$ will be separated along the y axis by 10 mm.

In Table Ia we give the possibilities of different accelerator complexes for obtaining radioactive beams by the fragmentation method. Figure 9 shows schematically the intensities of the radioactive beams in the fragment separator RIPS (RIKEN, Japan).

1.2. The ISOL method of producing radioactive beams

As already noted at the beginning of this section, this method uses the greatest possible thicknesses of the targets, which, as a rule, are placed in the ion source of the mass separator, and subsequent acceleration of the products of the nuclear reactions separated by the mass separator and transported to the postaccelerator (see Fig. 10). In connection with this, the ISOL method in principle surpasses the method of fragmentation of heavy ions in the intensity of the radioactive beam and also with regard to the energy resolution (Table Ib), which is determined by the resolution of the postaccelerator (for example, a tandem, Van der Graaff accelerator). In this case it is possible to vary the energy of the radioactive beam from a few tens of kilo-electron-volts (after the ion source) to several tens of mega-electron-volts (after the postaccelerator).

In this method of producing radioactive beams, the targets and ion sources must satisfy particular requirements. The target thickness (d) must be sufficiently great, and it must take a high intensity of the initial beam. At the same time, the target thickness must ensure a fairly rapid diffusion from it of definite elements. Table II gives data on the optimum target thicknesses and the maximum beam intensities of the various particles used to obtain radioactive nuclei by the ISOL method.

The thermal neutrons used to obtain radioactive beams in the PIAFE project (Grenoble, France) will have intensities of a few units per 10^{14} neutrons·cm^{-2}·s^{-1} for target thickness ~ 1 g/cm^2. The protons with energy 30 MeV used in the ARENAS project (Louvain-la-Neuve, Belgium) have, despite their short range, a mean intensity of ~ 500 μA. The power released in the target then exceeds 10 kW. For protons with energy 1 MeV in a ^{238}U target, a power of about 5 kW is released (at intensity 3 μA). In the ISOLDE project (CERN), it is proposed to use a target extended over 40 cm, which it is hoped can withstand a 30-fold increase in the intensity of the initial proton beam (up to 100 μA). Heavy ions have the greatest energy losses and, accordingly, highest densities of released power. Therefore one uses special materials for the target, as a rule, multilayer and situated within the source, as is planned for the project being developed at GANIL (France).

The next important problem is to transmit with minimum loss the nuclei produced in the target to the ion source. The efficiency of such a system is an important parameter and determines the coefficients $\varepsilon_{\text{extr}}$ and $\varepsilon_{\text{transport}}$ in the expression (1). The coefficient $\varepsilon_{\text{extr}}$ depends on the material of the target and the properties of the processes of diffusion and desorption from this material. Usually, the materials are chosen in such a way that $\varepsilon_{\text{extr}}$ is between 90% and 100%.[71] A high

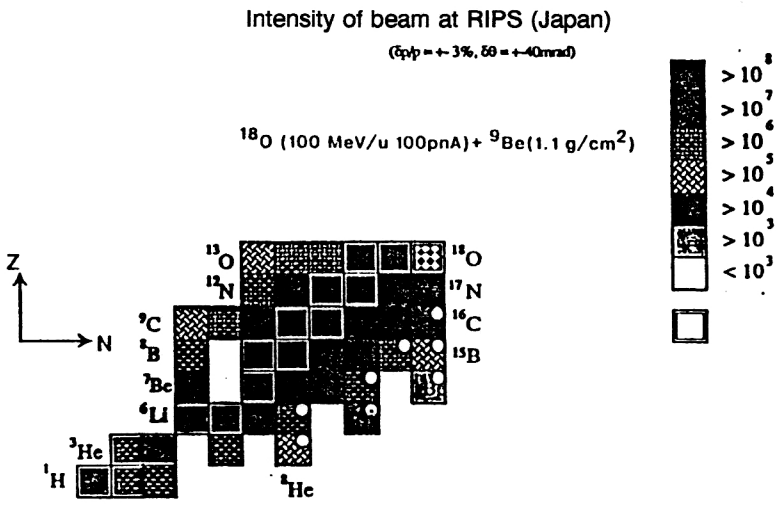

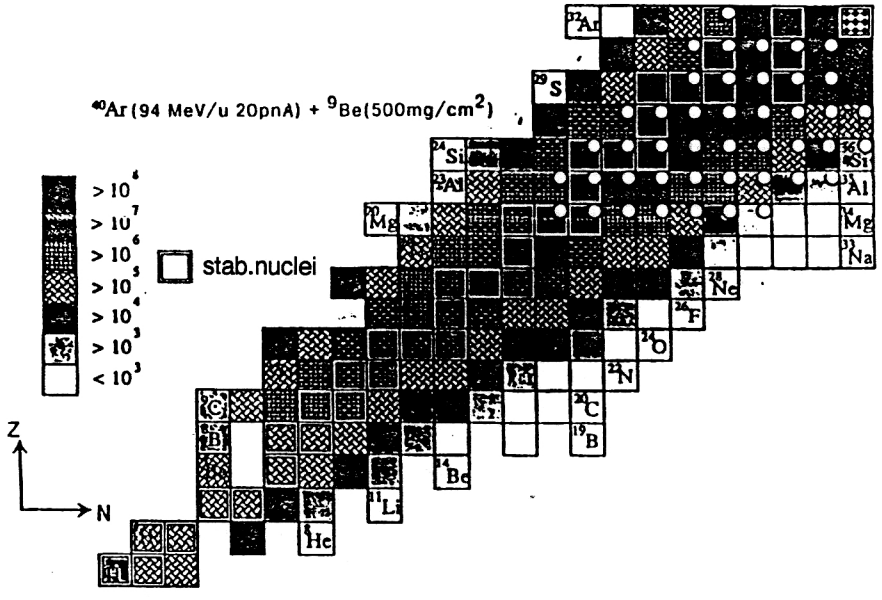

FIG. 9. The $N-Z$ diagram with intensity of radioactive beams obtained using the fragment separator RIPS (RIKEN, Japan) in the reaction $^{18}O+^{9}Be$ (upper figure) and $^{40}Ar+^{9}Be$ (lower figure) at ion energies ~100 MeV/A.

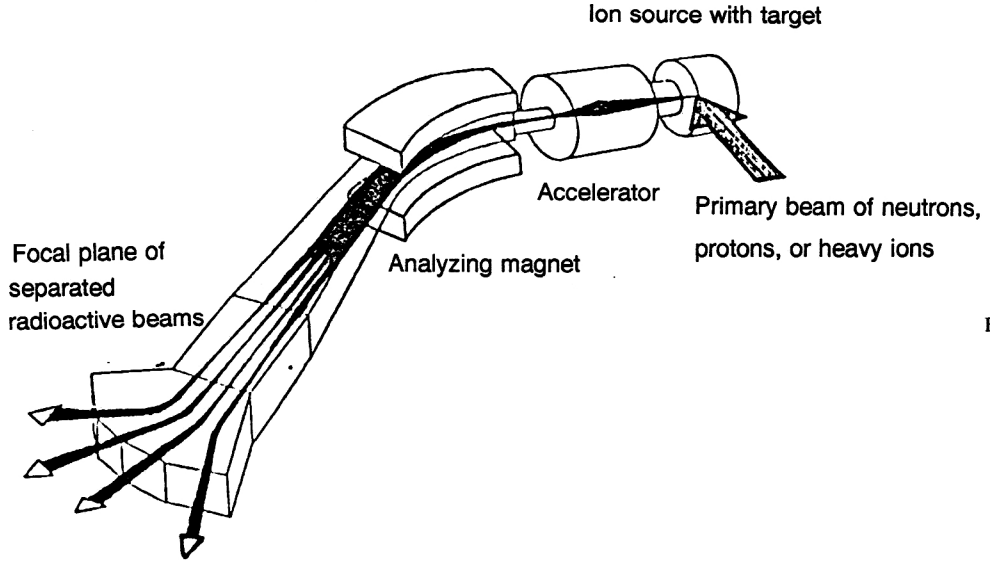

FIG. 10. One version of ISOL systems.

TABLE Ib. Accelerator facilities in combination with systems of ISOL type for the production of radioactive beams.

Facility	Accelerator for initial beam	Accelerator of secondary radioactive nuclei	A	E, MEV/A	I, s^{-1}	Status of facility
RIB, Louvain-la-Neuve, Belgium	Cyclotron K-30, $\leq$30 MeV H^-, $\leq$500 μA	Cyclotron K-110, CYCLONE	$\leq$20	$\leq$1.5	$\leq{}^{13}N{:}5\cdot10^8$ $\leq{}^{19}Ne{:}2\cdot10^8$	Operating
ARENAS, Belgium	Cyclotron K-30, $\leq$30 MeV H^{-1}, $\leq$500 μA	New cyclotron	$\leq$30	$\leq$1.5	$\leq10^9$	Plan
ORIB, ORNL, Oak Ridge, USA	Cyclotron K-105 ORIC, $\leq$75 MeV H^+, $\leq$52 MeV $^2H^+$, $^{3,4}He$,$^{6,7}Li$,^{10}B,$^{11}B\leq$70 μA	25 MB tandem	$\leq$80	$\leq$13	$\leq10^{11}$	The same
ISAC TRIUMF, Vancouver, Canada	Cyclotron TRIUMF, 500 MeV H^-, $\leq$10 μA	RFQ+LINAC	$\leq$60	$\leq$1.5	$\leq10^9$–10^{12}	*
E ARENA, Tokyo, Japan	LINAC, 1 GeV H^+, $\leq$10 μA	RFQ+LINAC	$\leq$120	$\leq$6.5	$\leq10^9$–10^{12}	*
PRIMA/ISOLDE, CERN, Geneva, Switzerland	PS booster, 1 GeV H^+, $\leq$9 μA	RFQ+LINAC	$\leq$27	$\leq$1.2	$\leq10^9$–10^{12}	Under construction
Moscow meson factory, Troitsk, Russia	LINAC, 800 MeV H^+, $\leq$1000 μA	RFQ+LINAC	$\leq$150	$\leq$6.5	$\leq10^9$–10^{12}	Plan
LSL, Los Alamos, USA	500–1000 MeV, light-ion accelerator $\leq$100–200 μA	RFQ+LINAC	$\leq$240	$\leq$10	$\leq10^9$–10^{12}	The same

transporting coefficient ($\varepsilon_{transport}$) is achieved by choosing materials of the target container, transport tube, and ion source that are similar as regards the chemical and thermal properties, the losses in these also being determined by the adsorption and diffusion. In addition, these elements must withstand high temperatures.

Exceptionally important for the obtaining of radioactive beams is the choice of a reaction having the largest cross section for production of the products. Three processes are used for reactions with protons—collision (spallation), fission, and fragmentation. The advantages of the various reactions for obtaining isotopes in different mass regions were analyzed by Rudstam.[16] Subsequently, reactions using high-energy (up to relativistic energies) light ions started to compete with these reactions.[17] Finally, for the regions of A corresponding to the maxima of the mass distributions of fission fragments ^{235}U fission by thermal neutrons proved to be very effective. Low-energy ($E<100$ MeV) protons leading to reactions of the type (p,n), $(p,2p)$, and (p,α) give a high yield of products near the stability line. However, it is only at proton energies $E>100$ MeV that the target nuclei undergo spallation and fragmentation reactions leading to the production of reaction products in wide ranges of Z and A. It is interesting that the cross sections for the production of these products in the range of proton energies from 200 MeV to 1 GeV hardly increase at all for masses of the products in the region of fragmentation or fission of the target nuclei (see Fig. 11).

However, for deep spallation reactions this dependence has a somewhat different form (see Fig. 12). Increase of the proton energy leads to a significant increase in the cross section of nuclei far from stability.

For spallation reactions leading to nuclei near the stability line, the maximum cross section is situated near the proton energy $\approx$900 MeV. With further increase of the proton energy, the target fragmentation channel is opened, and this leads to the production of neutron-rich nuclei (see Fig. 13). The existence of intense beams of heavy ions with energy near 30 MeV/A makes the fragmentation channel very promising for the production of nuclei far from the stability line. Comparison of the possibilities of the reactions with ^3He and ^{12}C ions and the spallation and fragmentation reactions on protons revealed an increase of the yield of isotopes far from the stability line in the heavy-ion reactions by a factor of at least 50. However, nuclei with mass $A\approx$88–98 have the greatest cross section in ^{235}U fission reactions induced by thermal neutrons. Figure 14 shows the isotope distributions of Rb produced in reactions with protons (E_p=40, 156 MeV, 1 GeV) and ions ^{12}C (77 MeV/A) and as fission fragments. One can see the advantage of heavy-ion reactions for masses $A\approx$80–88 and neutron-induced fission reactions for masses $A\approx$88–98. In the future, it may be very interesting to use the

TABLE II. Characteristics of beams of particles used to produce radioactive nuclei by the ISOL method.

Particle	Energy, MeV	Energy loss dE/dx, $MeV\cdot g^{-1}\cdot cm^{-2}$	Thickness of target, g/cm^2, element	Power released by beam with intensity $6\cdot10^{12}$ particles/s (1 μA), W	Power density, W/cm^3	Maximum achieved beam intensity, particles/s
Neutrons	thermal	160/fission	1,^{235}U	160	32	$5\cdot10^{14}$
Protons	1000	1.2	110,^{238}U	420	7	$6\cdot10^{14}$
Protons	30	16.7	0.9,^{12}C	30	75	$3\cdot10^{15}$
^{12}C	1152	200	4,^{120}Sn	800	1200	$6\cdot10^{13}$
^{36}Ar	3456	2351	0.9,^{12}C	2100	5250	$6\cdot10^{13}$

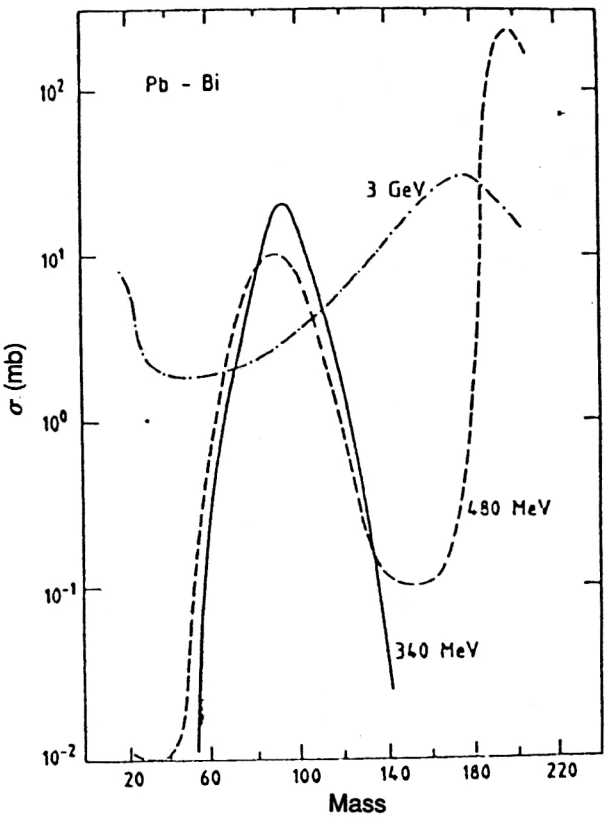

FIG. 11. Mass distribution of reaction products produced by bombarding Pb and Bi with protons of different energies.

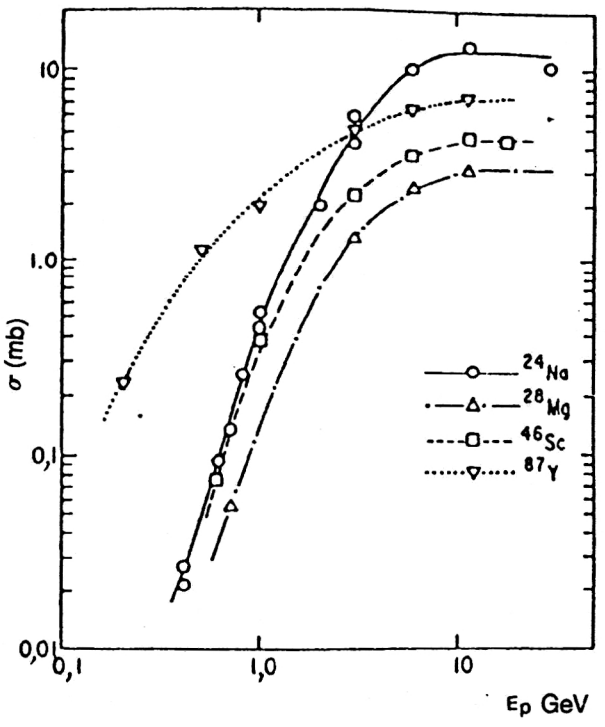

FIG. 13. Excitation function for different isotopes produced in gold fragmentation reactions.

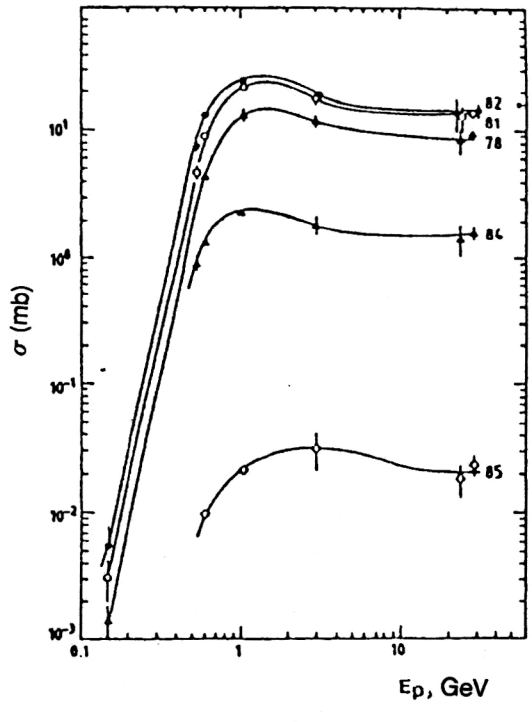

FIG. 12. Excitation function of krypton isotopes produced in spallation reactions on a silver target ($\Delta Z=11$).

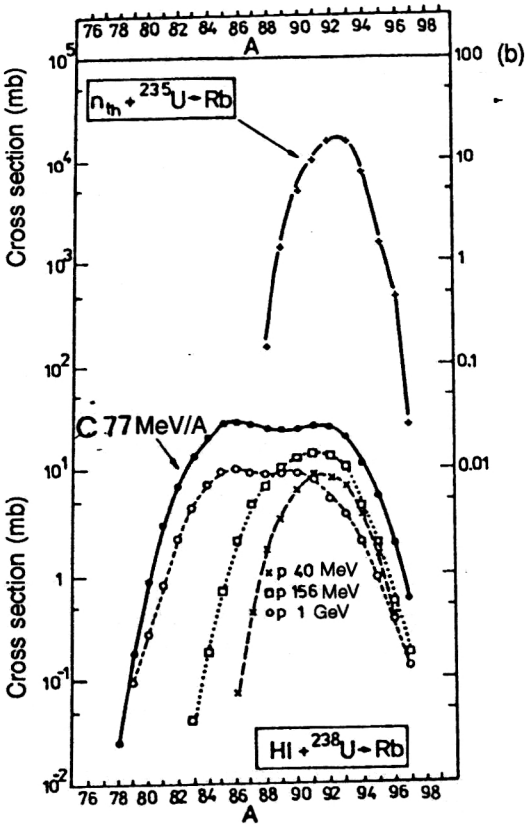

FIG. 14. Cross section for the production of rubidium isotopes in various reactions.

TABLE III. Comparison of yields of radioactive nuclei after targets using a beam of protons at the ISOLDE facility at CERN and using heavy ions at the accelerator facility GANIL (France).

	CERN — ISOLDE				GANIL				
	Reaction	Target thickness, g/cm^2	Yield of nuclei (1 s/10 μA)	$T_{1/2}$	Reaction	Target thickness, g/cm^2	σ, mb	Coefficient of increase	Yield of nuclei (1 s/10 μA)
^{8}He	Th + p	56	$8\cdot10^{9}$	119 ms	^{11}B + ^{12}C	2,5	10	10	$6\cdot10^{10}$
^{8}Li	Ta + p	122	$4\cdot10^{10}$	842 ms	^{10}B + ^{12}C	3,5	25	4	$2{,}5\cdot10^{11}$
^{9}Li	Ta + p	122	$1{,}5\cdot10^{10}$	173 ms	^{11}B + ^{12}C	2,5	8	4	$6\cdot10^{10}$
^{11}Li	Ta + p	122		8,7 ms	^{18}O + ^{12}C	1,3	0,01	1,5	$4\cdot10^{7}$
^{7}Be	C + p	30		53 days	^{9}B + ^{12}C	4	23	4	$2{,}9\cdot10^{11}$
					^{10}B + ^{12}C	3,5	19	4	$2\cdot10^{11}$
^{11}Be	Ta + p	122	$1{,}5\cdot10^{10}$	13,8 s	^{13}C + ^{12}C	2	5	2	$3\cdot10^{11}$
^{14}Be				4 ms	^{18}O + ^{12}C	1,3	0,0025	1,5	$1\cdot10^{7}$
^{9}C				127 ms	^{12}C + ^{12}C	2,5	2·0,3	3	$4{,}7\cdot10^{9}$
^{16}C	^{18}O + p	6	$1{,}3\cdot10^{10}$	750 ms	^{18}O + ^{12}C	1,3	0,5	4	$2\cdot10^{9}$
^{18}C					^{22}Ne + ^{12}C	1,1	10^{-2}	4	$3\cdot10^{7}$
^{13}N	^{16}O + p	2	$5\cdot10^{10}$	10 min	^{14}N + B	2,2	50	2	$3\cdot10^{11}$
^{14}O	^{14}N + p	10		70,5 s	^{16}O + ^{12}C	1,9	2	4	$1{,}3\cdot10^{10}$
^{19}Ne	^{24}Mg + p	3	$3{,}6\cdot10^{10}$	17,2 s	^{20}Ne + ^{12}C	1,4	50	2	$2{,}2\cdot10^{11}$
^{21}Ne	Ti + p	40	$9\cdot10^{10}$	22,5 s	^{23}Na + ^{12}C	1,2	30	4	$1\cdot10^{11}$
^{29}Ne	U + p	13	$4\cdot10^{6}$	43 s	^{12}C + U	4,0	10^{-2}	1,5	$6\cdot10^{6}$
					^{40}Ar + ^{12}C	9	$5\cdot10^{-2}$ 3	2	$1{,}4\cdot10^{7}$
^{46}K	U + p	13	$9\cdot10^{7}$	1,8 min	^{12}C + U	4,0	5	1,5	$3\cdot10^{8}$
					^{12}C + ^{48}CaO	4	20	4	$3\cdot10^{10}$
^{72}Zn	Ge + p	134	$1{,}6\cdot10^{7}$ (b)	46 h	^{12}C + Au	4,9	20	2	$2\cdot10^{10}$
^{80}Rb	Nb + p	50	$1{,}9\cdot10^{11}$	30 s	^{12}C + U	4,0	0,7	1,5	$4\cdot10^{8}$
					^{12}C + ^{93}Nb	3,5	1,8	3	$2{,}5\cdot10^{9}$
^{83}Rb	Nb + p	50	$1{,}5\cdot10^{11}$	86,2 days	^{12}C + U	4,0	12	1,5	$7{,}6\cdot10^{9}$
					^{12}C + Nb	3,5	15	2	$2\cdot10^{10}$
^{97}Rb	U + p	13	$1{,}2\cdot10^{8}$	170 ms	^{12}C + U	4,0	0,6	1,5	$3{,}8\cdot10^{8}$
^{119}Cs	Ta + p	122	$1{,}3\cdot10^{4}$ (c)	44 s	^{12}C + Ta	4,5	0,04	1,5	$4\cdot10^{7}$
	La + p	150	$1{,}4\cdot10^{9}$		^{12}C + La	4,4	1,6	10	$1{,}5\cdot10^{9}$
^{130}Cs	U + p	13	$5\cdot10^{10}$	29,9 min	^{12}C + U	4	12	1,5	$9\cdot10^{9}$
		13	$1{,}6\cdot10^{10}$ (d)						
^{145}Cs	U + p	13	$2\cdot10^{8}$	59 s	^{12}C + U	4	0,3	1,5	$2\cdot10^{8}$

heavy-ion fragmentation reaction to obtain strongly neutron-rich or neutron-deficient isotopes (SPIRAL project). Thus, in planning experiments with radioactive beams, it is necessary to estimate their yield in particular reactions, this largely determining the intensity of the secondary beams [see (1)].

1.3. Facilities using the ISOL method to obtain radioactive beams

Facilities to produce beams of radioactive nuclei are currently being developed in practically all the leading nuclear physics centers in the world. In the first place, projects using the ISOL method are ARENAS-3 (Louvain-la-Neuve, Belgium), EXCYT (Catania, Italy), CERN-ISOLDE (Switzerland), SPIRAL (Caen, France), PIAFE (Grenoble, France) in Europe and also projects at Oak Ridge (United States) and at Vancouver (Canada).

Table III gives the parameters of the facilities being developed to produce beams of radioactive nuclei by the ISOL method. We give below a brief description and the main characteristics of the facilities that, in our view, are the most

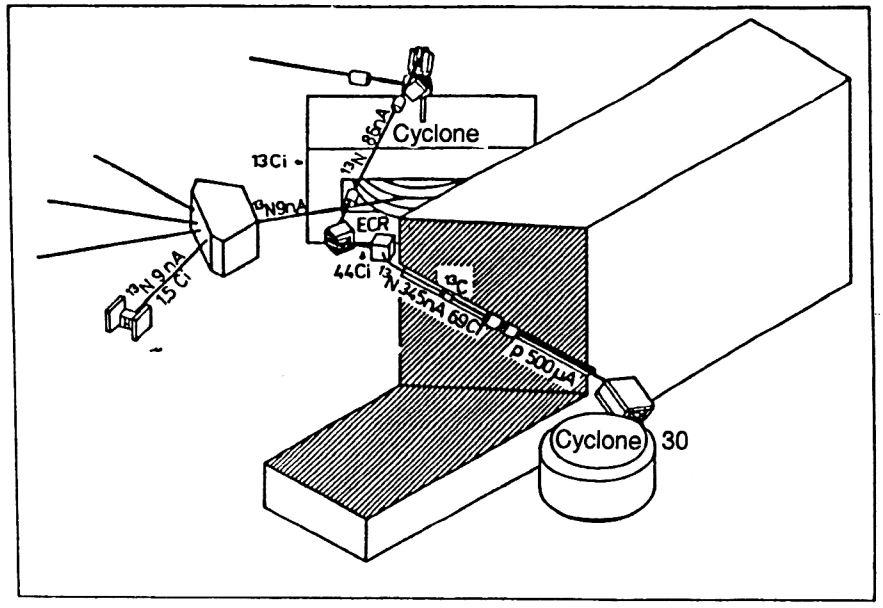

FIG. 15. Schematic representation of the facility ARENAS. The intensities of the radioactive ^{13}N beam in the (^{13}C, p) reaction are shown.[11]

promising for the production of radioactive beams by the ISOL method.

ARENAS is an operating facility for the production of radioactive beams at Louvain-la-Neuve (Belgium).[19] The method is based on the use of two cyclotrons to produce and accelerate radioactive nuclei (see Fig. 15). The first cyclotron CYCLONE-30 accelerates the protons to energy 30 MeV and intensity $I \leqslant 500$ μA. For further acceleration of the radioactive nuclei, a cyclotron with variable energy ($K=110$ MeV) is used. The maximum energy of the nuclei accelerated in this cyclotron is $E_{max} \leqslant 110 q^2/A$ (q is the charge of the ion, and A is its atomic number). The produced reaction products [currently the (p,n), $(p,2n)$, (p,pn), and (p,α) reactions are mainly used] are ionized in a ECR source to charges from 1^+ to 4^+ and are then accelerated in the second cyclotron to energies 0.56–27 MeV/nucleon (minimum $A/q=13$ and maximum $A/q=2$). The coefficient of transmission from the target to the ion source in this facility is an important factor that determines the maximum intensity of the beams of radioactive nuclei and is $I_{transport}/I_{source}=0.03$–$0.08$. Investigations with a restricted number of radioactive nuclei (^{13}N,^{19}Ne,^{11}C) are currently being made with ARENAS. However the project ARENAS-3, which is being developed for commissioning in 1997 and includes a new postaccelerator with $K=33$, will make it possible to extend considerably the range of radioactive nuclei and to carry out investigations with neutron-deficient nuclei with $A \leqslant 40$, the intensity of which will be 10^8–10^9 particles/s.

CERN-ISOLDE is an on-line separator of the CERN synchrocyclotron with proton energy 600 MeV. This facility has been operated since 1967 up to the present day and is distinguished by a high intensity of the beams of radioactive nuclei in the range $Z=1$–91 and a high mass resolution (~30 000). The characteristics of the secondary ISOLDE beams are given in Table III. It can be seen that at this facility some nuclei can be obtained with intensity 10^7–10^8 particles/s. A project for producing beams of accelerated radioactive nuclei at CERN includes as generator of the beams of radioactive nuclei the CERN PS-Booster (synchrotron) with energy 1 GeV and intensity 2 μA. This project will be realized in collaboration with the Rutherford Laboratory (RAL, Great Britain), which has great experience in the development and construction of high-intensity sources of neutrons and protons with intensity up to 200 μA and also of targets that can withstand a high power of the primary beams.[22]

At the present time the type of postaccelerator for the CERN-ISOLDE project is under discussion. It will either be a RFQ or a superconducting LINAC with intermediate beam stripping. The postaccelerator will be used to accelerate ions with charge $q=1^+$ and maximum energy 5 MeV/nucleon for ions with $A \leqslant 80$.

The SPIRAL project is a development of the accelerator facility GANIL, at which beams of radioactive nuclei with intensity up to 10^6 particles/s and energy 30–90 MeV/nucleon are currently obtained by the fragment-separator method.[21] The accelerator complex of GANIL currently consists of three cyclotrons, two of which function in a tandem regime. The maximum energy of the accelerated heavy ions is 100 MeV/nucleon for $q/A=0.5$. The SPIRAL project, which will be realized in 1994–1997, includes the old accelerator complex. Beams of accelerated heavy ions will bombard a target placed within a ECR source of multiply charged ions (see Fig. 16). After magnetic analysis, the separated products of the nuclear reactions will be injected and accelerated by means of a compact cyclotron with $K=262$ MeV to energy 2.6 MeV/nucleon for $q/A=0.1$ and 29 MeV/A for $q/A=0.5$. Significant progress in the technology of the ECR sources (for the light ions ^3He and ^{12}C, an intensity of $5 \cdot 10^{13}$ particles/s was obtained) makes it possible to hope that this project will become one of the most promising for the study of intense beams of radioactive nuclei of intermediate energies (see Table III).

PIAFE is a new original project for obtaining intense beams of radioactive nuclei in the region of the maximum yield of fragments of thermal-neutron-induced ^{235}U fission

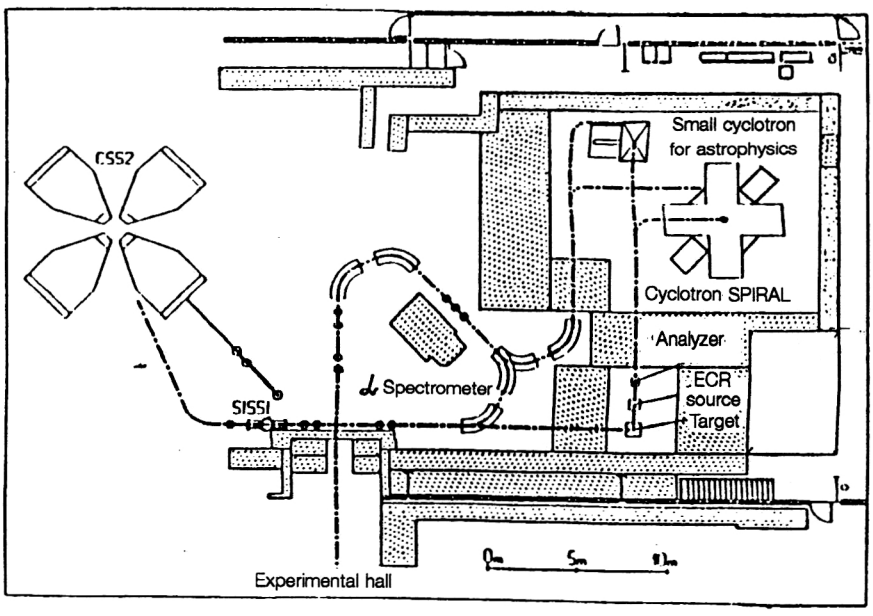

FIG. 16. Scheme for producing radioactive beams at the accelerating facility GANIL (SPIRAL project).

(Kr and Xe).[11] It is proposed to use the high-current reactor of the Laue-Langevin Institute at Grenoble with beam power in the core, where the target will be placed, up to $1 \cdot 10^{14}$ neutron$\cdot$cm$^{-2}\cdot$s^{-1}. The radioactive products will then be sent to an ion source situated at a certain distance from the target, where they will be ionized once (see Fig. 17), after which the nuclei separated by means of a separator will be injected into the SARA accelerator complex (Institute of Nuclear Research, Grenoble), which is 400 m from the reactor. Secondary ionization of the radioactive nuclei will be done by means of the ECR source of the first injector of the SARA complex. The accelerator complex consists of two cyclotrons—a compact injector with $K=88$ MeV and a postaccelerator in the form of a cyclotron with separated sectors with $K=160$ MeV. This system will make it possible to obtain nuclei in the mass range $A\sim 75$–150 with energy 2–10 MeV/nucleon (for the mass $A=80$, possibly up to 20 MeV/nucleon) and with high intensity (see Table IV).

Among the interesting projects for using radioactive beams we may mention the EXCYT project of the National Laboratory for Heavy-Ion Physics at Catania (Italy) and also the PSI project (Paul Scherer Institute, Germany). In the first case, it is proposed to use as postaccelerator a 15 MV tandem, which will make possible a high energy resolution of the secondary beam; in the second case, the high-intensity primary beam of protons (up to 1.5 mA) with energy 590 MeV will make it possible to obtain beams of radioactive nuclei with intensity up to 10^8 particles/s and energy up to 30 MeV/A.

All these projects are being realized in Europe. With regard to American projects, the most promising are the project at the Oak Ridge National Observatory, which includes an isotope separator (ISOL) with target to produce proton-rich isotopes in reactions of complete fusion with light ions[23] accelerated in an isochronous cyclotron (ORIC). After the separator, the positively charged ions are converted

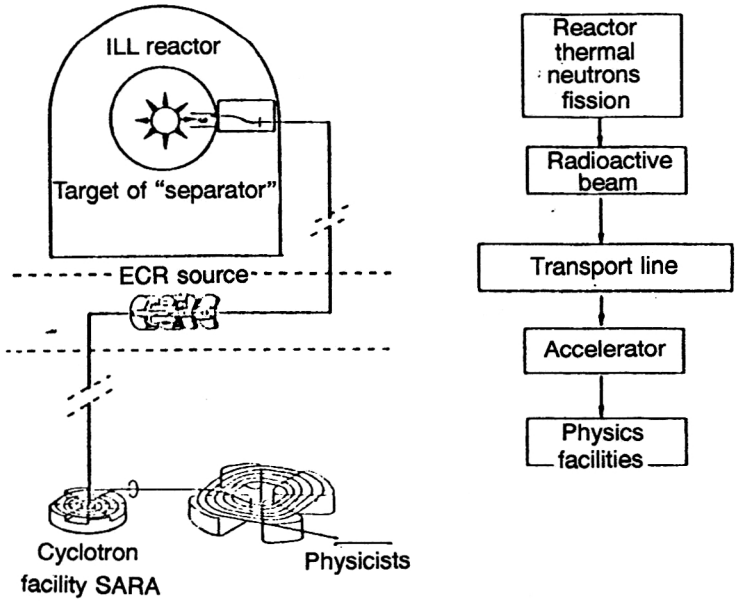

FIG. 17. Schematic diagram of production of radioactive nuclei in the project PIAFE (Production, Ionization, Acceleration of Exotic Beams Facility) (Grenoble, France).

TABLE IV. Planned intensity of beams of radioactive nuclei at various European projects.

Beam	$T_{1/2}$	ISOLDE	GANIL SPIRAL	CATANIA	ARENAS-3		PIAFE	PSI
					k = 30	k = 110		
		Intensity, Atom·s^{-1}·μA^{-1}	Intensity, Atom·s^{-1}·μA^{-1}	Intensity, Atom·s^{-1}·μA^{-1}	Intensity, Atom·s^{-1}·μA^{-1}	Intensity, Atom·s^{-1}·μA^{-1}	Intensity, Atom·s^{-1}·μA^{-1}	Intensity, Atom·s^{-1}·μA^{-1}
^{8}He	122 ms	2,6E+8	2,2E+6				,	
^{8}Li	842 ms	1,1E+9	1,6E+9	1,6E+9		4,2E+9	,	
^{11}Li	9 ms	1,5E+4	6,1E+4	6,1E+4			,	
^{7}Be	53 days	1,4E+10	1,4E+8		7,5E+7	1,7E+8		1,9E+7
^{14}Be	5 ms	2,8E+2	2,2E+0				,	
^{11}C	20 min	9,3E+9	1,5E+9	1,5E+9	7,5E+8	1,8E+9		1,3E+8
^{13}N	10 min	7,0E+9	3,8E+9	3,8E+9	1,6E+9	2,2E+9	,	
^{14}O	71 s	2,9E+9	5,3E+8	5,3E+8		4,4E+8	,	
^{15}O	2 min	4,3E+9	2,9E+9	2,9E+9	5,7E+8	1,8E+8	,	
^{19}O	27 s	1,4E+9	3,3E+8	3,3E+8			,	
^{22}O	2,3 s	3,0E+6	6,1E+4	6,1E+4			,	
^{17}F	65 s	1,6E+8	5,8E+7	5,8E+7				1,0E+8
^{19}Ne	17 s	2,3E+10	2,1E+9		7,0E+8	1,5E+9	,	
^{26}Ne	162 ms	1,1E+6	3,1E+5				,	
^{20}Na	446 ms	9,8E+8	5,7E+8	5,7E+8			,	
^{30}Na	53 ms	1,3E+4	3,5E+3	3,5E+3			,	
^{26m}Al	6 s	1,9E+6	1,2E+8				,	
^{30}S	1 s	5,0E+2	1,2E+3	1,2E+3			,	
^{34}Ar	844 ms	2,3E+8	4,0E+8		1,8E+8	3,4E+8	,	
^{35}Ar	1,8 s	2,4E+9	2,2E+9		7,0E+8	1,4E+9	,	
^{72}Zn	46 h	2,2E+8	2,7E+7					1,2E+6
^{78}Zn	1,5 s	1,1E+6	1,7E+5				2,2E+5,	
^{73}Se	7 h	8,3E+9	3,2E+8					1,1E+6
^{74}Kr	12 min	1,6E+9	9,8E+7				,	
^{91}Kr	8,6 s	1,2E+9	1,7E+8		4,4E+7		1,5E+12,	
^{94}Kr	0,2 s	1,1E+7	3,1E+6				1,8E+9,	
^{97}Rb	170 ms	9,6E+7	5,3E+7				2,6E+9,	
^{111}In	2,8 days	1,8E+10	1,2E+9					8,1E+5
^{105}Cd	56 min	8,0E+8	2,0E+7					1,1E+6
^{108}Sn	10 min	2,9E+7	5,4E+6					3,5E+4
^{132}Sn	40 s	3,5E+6	6,3E+5				1,9E+8	2,8E+4
^{121}Cs	2,3 min	2,2E+10	6,2E+8					1,6E+5
^{144}Cs	1 s	8,2E+9	1,5E+9				2,5E+9,	
^{142}Xe	1,2 s	3,3E+7	6,1E+6				1,5E+11,	
^{144}Xe	1,2 s	7,0E+5	1,3E+5				2,6E+9,	

into negative ions by the method of direct surface ionization. After preacceleration to 300 keV, the negatively charged ions are injected into a tandem accelerator with energy 25 MeV for subsequent acceleration. Beams with mass up to $A=80$ will have energy 5 MeV/nucleon. For some radioactive beams, the intensity will reach 1 nA at beam intensity of the ORIC cyclotron of 0.5 kW (see Table V).

Figure 18 shows the possibilities of the various complexes for producing radioactive nuclei in different energy ranges. All these projects are in the stage of realization, and therefore it will be three or four years before physics experiments are begun at them; on the other hand, the facilities that use the fragment-separation method are already being used in experiments.

1.4. Production of beams of radioactive nuclei in reactions with low-energy heavy ions

Reactions with radioactive beams near the Coulomb barrier are of great interest for physics investigations. Processes such as below-barrier fusion, transfer reactions, and low-energy fission can be investigated only at energies near

TABLE V. Planned intensity of radioactive nuclei at the Oak Ridge facility for the production of radioactive beams (USA).[23]

Isotope	Intensity, ion/s	Maximum energy, MeV/A	Isotope	Intensity, ion/s	Maximum energy, MeV/A
^{10}C	$4{,}3\cdot10^{7}$	13,0	^{83}Ga	$1{,}5\cdot10^{5}$	6,1
^{11}C	$5{,}0\cdot10^{7}$	13,0	^{84}Ga	$1{,}5\cdot10^{6}$	6,0
^{14}O	$1{,}4\cdot10^{8}$	13,0	^{68}As	$1{,}1\cdot10^{9}$	5,9
^{15}O	$3.3\cdot10^{8}$	13,0	^{68}As	$1{,}3\cdot10^{9}$	5,9
^{17}F	$1{,}1\cdot10^{10}$	12,7	^{70}As	$1{,}0\cdot10^{9}$	5,8
^{18}F	$5{,}8\cdot10^{9}$	12,3	^{70}Se	$1{,}9\cdot10^{8}$	5,8
^{21}Na	$4.3\cdot10^{7}$	11,2	^{71}Se	$9{,}3\cdot10^{7}$	5,7
^{22}Na	$4{,}3\cdot10^{7}$	10,7	^{72}Se	$1{,}9\cdot10^{8}$	5,6
^{28}Si	$1{,}2\cdot10^{9}$	8,8	^{74}Br	$3{,}3\cdot10^{7}$	5,5
^{27}Si	$1{,}0\cdot10^{9}$	8,8	^{75}Br	$1{,}7\cdot10^{7}$	5,3
^{33}Ci	$2{,}5\cdot10^{10}$	7,8	^{77}Br	$6{,}8\cdot10^{6}$	5,3
^{34}Ci	$2{,}2\cdot10^{10}$	7,5	^{77}Rb	$1{,}4\cdot10^{5}$	5,3
^{37}K	$6{,}5\cdot10^{6}$	7,0	^{78}Rb	$1{,}2\cdot10^{6}$	5,2
^{38}K	$3{,}3\cdot10^{7}$	6,8	^{79}Rb	$1{,}2\cdot10^{5}$	5,2
^{58}Cu	$1{,}0\cdot10^{9}$	6,3			

$E/B_{Coul}\approx1$. However, the production of intense beams of radioactive nuclei at such energies becomes problematic because of the impossibility of using thick targets, and also because of the relatively broad angular distribution of the secondary products of these reactions. In some laboratories that use fragmentation reactions to produce radioactive beams, the beams are "cooled" by means of various methods, which range from simple absorption in foils to deceleration.[24] However, the quality of radioactive beams (energy resolution, angular distribution, intensity) is in all these cases insufficient for high-precision measurements. Therefore, in a number of centers in which there are accelerators of heavy ions with energy $E=10$ MeV/nucleon reactions at these energies are used to produce mainly nuclei of the light elements (He, Li, Be) with energies near the Coulomb barrier. These reactions—nucleon stripping, charge exchange, few-nucleon transfer, nonequilibrium emission, knockout, etc.—have fairly high cross sections, up to several hundred millibarns, and relatively narrow angular distribution, and this makes it possible to obtain beams of radioactive nuclei such as ^{6}He,^{8}Li,^{7}Be,^{17}F,^{15}O, etc., up to 10^{6} particles/s. Table VI presents the results of recent experiments on the production of low-energy radioactive beams. Although the employed reactions can produce a number of radioactive nuclei that is rather restricted as regards Z and A, the intensity and energy resolution make it possible to use them in investigations of the characteristics of exotic reactions and also to produce and study the properties of exotic nuclei (for example, $^{2}H(^{7}Be,^{8}B)$.

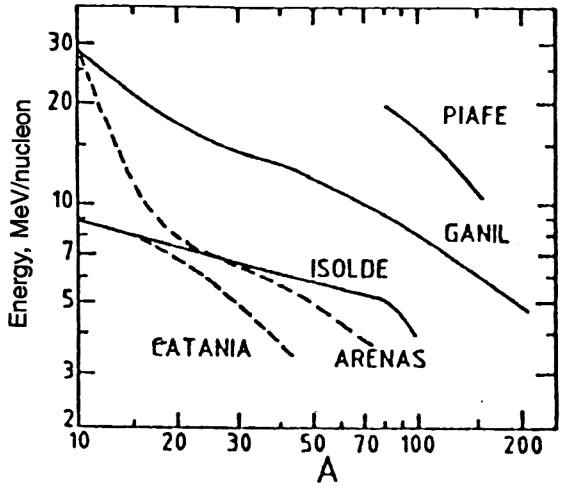

FIG. 18. Comparison of possibilities of producing radioactive beams with mass A with different energies in facilities using the ISOL method.

1.5. Storage rings for investigations with radioactive beams

New possibilities using beams of radioactive nuclei are opened up by the commissioning of storage rings with electron cooling.[25] Such storage rings are currently used to produce heavy-ion beams (see Table VII).

The ESR storage ring at Darmstadt, which has been functioning since 1990, is currently used to form beams of radioactive nuclei.[26] It operates in the storage-ring regime with injection into it of a heavy-ion beam from a synchrotron (SIS), and also in the storage–cooling regime with a beam of completely stripped radioactive nuclei obtained in fragmentation reactions and separated in the fragment separator (FRS), which in the given case is also the injector of the storage ring. In the storage ring, which makes it possible to obtain beams of radioactive nuclei with energy up to 0.5–1

TABLE VI. Possibilities of different facilities for obtaining radioactive beams of low energies.

Laboratory, country	Accelerator	Separation method, maximum energy, solid angle	Intensity of secondary beam	Reaction	Energy and resolution, MeV	Investigated reactions with secondary beams
UND/UM, USA	FN, tandem	Superconducting solenoid, 3 MeV/A, 160 msr	^{8}Li 1.2·10^{6} ^{6}He 5·10^{4} ^{7}Be 2·10^{4} ^{18m}F 2·10^{3}	^{9}Be(^{7}Li,^{9}Li) ^{9}Be(^{7}Li,^{6}He) ^{1}H(^{10}B,^{7}Be) ^{10}B(^{6}Li,^{7}Be) ^{12}C (^{16}O,^{18m}F)	^{8}Li 13–20±0.5 ^{6}He 8–10±0.7 ^{7}Be 9–22±0.9 ^{18m}F 55±2.1	^{197}Au,Ti,^{27}Al, C,^{9}Be (^{6}He,^{6}He) CD_2,Be,C (^{8}Li,^{8}Li) ^{12}C(^{8}Li,^{8}Li*)
CIAE, China	HI-13, tandem	GIRAFFE DQQ mag., 6 MeV/A, 2 msr	^{7}Be 1·10^{7} ^{8}Li 1·10^{6} ^{11}C 4·10^{6} ^{17}F 1·10^{7}	^{1}H(^{7}Li,^{7}Be) ^{2}H(^{7}Li,^{8}Li) ^{1}H(^{11}B,^{11}C) ^{2}H(^{16}O,^{17}F)	^{7}Be 33±1 ^{8}Li 40±0.5 ^{11}C 60±1 ^{17}F 85±1.3	^{2}H(^{7}Be,^{8}B) ^{2}H(^{8}Li,^{9}Li) ^{2}H(^{11}C,^{12}N) ^{1}H(^{17}F,^{14}O)
LLNL, USA	EN, tandem	QSBTS system, 1.2 msr	^{7}Be 10^{4} ^{13}N	^{1}H(^{7}Li,^{7}Be) ^{2}H(^{12}C,^{13}N)	^{7}Be 18.6±0.5 ^{13}N 36±1.6	^{2}H(^{7}Be,^{7}B)
ANL, USA	ATLAS linear accelerator	ATLAS	^{17}F 8·10^{6}	^{1}H(^{17}O,^{17}F)	^{17}F 70±5	^{1}H(^{17}F,^{14}O)
RNCR, Japan	Cyclotron	DUMAS 1.2 msr	^{7}Be 2·10^{4}	^{1}H(^{7}Li,^{7}Be)	^{7}Be 140±2	^{2}H(^{7}Be,^{8}B) ^{12}C(^{7}Be,^{7}Be)
Tohuku U., Japan	Accelerator	magnet	^{15}O 10^{4}	^{1}H(^{15}N,^{15}O)	^{15}O 80	Pb(^{15}O,^{15}O)
JINR, LNR, Dubna, Russia	U-400M Accelerator	magnet, 10 msr	^{6}He,10^{6}	^{7}Li(Ta,^{6}He) ^{7}Li(^{1}H,2p)	^{6}He 90±1	^{209}Bi(^{6}He,f)

MeV/nucleon and energy resolution down to 10^{-4} (for example, FWHM of 42 keV at the 306-MeV level) a broad program of physics investigations is already realized—atomic physics with beams of completely stripped nuclei, nuclear reactions in inverse kinematics of light internal targets, measurement of masses of nuclei near the boundaries of nuclear stability, and more.

One of the most widely used methods of storing radioactive nuclei in storage rings is to cool them. This exploits the sharp reduction in the emittance of a beam injected into orbit as a result of electron cooling. The part of the orbit that is then made free can be used for subsequent injections of nuclei from a corresponding injector. If the velocity of the electrons in the storage ring is made equal to the mean velocity of the injected ions, the beam cooling time will be minimal and will be determined by the following expression for the transverse and longitudinal directions:

$$\tau_{\perp} \cong 2\cdot 10^{7}\,\frac{\beta^{4}\gamma^{5}(\varepsilon_{x,z}/\pi)^{3/2}}{q j_{e}\beta_{x,z}^{3/2}}\,\frac{A}{Z^{2}} \tag{17}$$

$$\tau_{\parallel} \cong 2\cdot 10^{7}\,\frac{\beta^{4}\gamma^{5}(\Delta P/P)^{3}}{q j_{e}}\,\frac{A}{Z^{2}}, \tag{18}$$

where $\beta=v/c$ and $\gamma=1/(1-\beta^{2})^{1/2}$, $\varepsilon_{x,z}$ is the transverse emittance of the injected beam in meters, q is the ratio of the length of the electron-cooled section to the perimeter of the beam orbit, j_e [A/cm^2] is the density of the electron beam, $\beta_{x,z}$ are the amplitude functions of the ring in the region of the electron cooling measured in meters, A and Z are the mass number and atomic number of the injected nuclei, and P and ΔP are the momentum and increment.

In the section of electron cooling, the values of β_x or β_z are ~10 m. For such values of the amplitude functions, the transverse sections of the electron beam are small, and this makes it easier to obtain a high electron density, which may be 0.1 A/cm^2. If the electron energies are taken equal to 15 keV, it is possible to obtain values of $\tau_{\perp}$ and $\tau_{\parallel}$ in the range 5–10 ms. This is the minimum beam cooling time. In the case of multiple repetition of injection events, a cooled beam can be stored in a stationary rf separator. The number of ions trapped in the separator is limited by two factors: first, the

TABLE VII. Comparison of parameters of storage rings with electron cooling.[25]

Facility	TSR	ASTRID	ESR	CRYRING
Laboratory	MPI	Univ.	ESI	MSI
Town	Heidelberg	Aarhus	Darmstadt	Stockholm
Country	Germany	Denmark	Germany	Sweden
Length, m	55.4	40	108.4	51.6
Experiment. length, m	3.8	3.0	9	2.7; 2.7
Magnetic rigidity, T·m	1.5	2.0	10.0	1.4
Electron energy, keV	12(20)	(2.5)	95(330)	
Start of experiments:				
Electron cooling	November, 1988		May, 1990	-
laser cooling	1989	May, 1990	-	-
Particles:				
main	C,H,Li^{+},Be^{+},	Ar,Li^{+}	Ar(Ne-U)	P(Ne,Kr)
other	O,Si,S,Cu(1)	electrons		
injectors	Tandem	Microtron separator (tandem)	Synchrotron fragment separator	RFQ CRYSIS

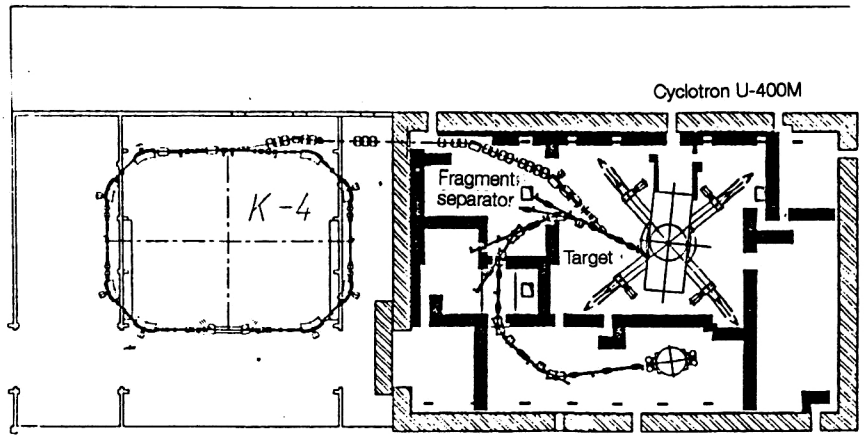

FIG. 19. Scheme of first stage of the storage ring K4 of the Flerov Laboratory of Nuclear Reactions, JINR, at Dubna.

beam instability due to space charge, second the gradual increase in the fraction of the orbit occupied by the stored beam. This effect is proportional to $N_i^{1/3}$, where N_i is the number of ions in the bunch. The calculations made in Ref. 27 show that the maximum number of ions that can be stored and kept in orbit does not exceed $4 \cdot 10^9$. The total time of storage and cooling of such a number of ions will be 170 ms. To a large degree, these values determine the possibilities of using storage rings in investigations with beams of radioactive nuclei (limitation on the cross section and lifetime).

Projects are currently being discussed for storage rings for radioactive beams at Legnaro (Italy) (22.5 T·m) (Ref. 28) and K4/K10 at Dubna.[29] The Dubna project includes two rings with electron cooling, the injector for which can be the high-current heavy-ion cyclotron U-400M. In the first stage of realization of the project, it is proposed to create the one ring K4, in front of which there will be a generating target, and a separating channel to obtain and inject the radioactive nuclei into the ring (Fig. 19). The possibilities of the ring K4 for the production of radioactive beams are presented in Table VIII.

2. EXPERIMENTAL INVESTIGATIONS WITH BEAMS OF RADIOACTIVE NUCLEI

When heavy-ion beams were first used, they made it possible to obtain new results in the study of nuclear structure and the mechanism of nuclear reactions. Nuclear reactions with heavy ions made it possible to synthesize new nuclei at the boundaries of nuclear stability, including the nuclei of new elements with $Z>100$. The appearance of beams of radioactive nuclei makes it possible to obtain and study nuclei in states with extremal isospin values. This makes it possible to progress significantly in understanding the traditional directions of heavy-ion physics: 1) the synthesis of new nuclei and the study of their properties and structures, which, as the first experiments with radioactive beams already showed, can be very different from the properties

TABLE VIII. Planned characteristics of the storage ring K4 of the Flerov Laboratory of Nuclear Reactions, JINR.

Beam	$T_{1/2}$, s	Injection energy, MeV/nucleon	Maximum energy, MeV/nucleon	Luminosity, $s^{-1} \cdot cm^{-2}$	$\lvert N - N_{\Delta N} \rvert$
^{6}He	0,808	104	176	10^{27}	2
^{8}He	0,122	109	123	10^{25}	0
^{9}Li	0,178	108	176	10^{27}	2
^{11}Li	0,009	109	121	10^{24}	0
^{11}Be	13,8	126	207	10^{27}	3
^{14}Be	0,05	120	132	10^{22}	0
^{12}B	0,02	85	264	10^{28}	5
^{17}B	0,006	121	139	10^{22}	0
^{16}C	0,75	114	219	10^{26}	2
^{18}C	0,1	122	176	10^{23}	0
^{14}O	70,6	109	456	10^{28}	2
^{22}O	0,76	118	207	10^{24}	2
^{24}Ne	225	126	264	10^{28}	8
^{28}Ne	0,014	121	200	10^{23}	2
^{44m}Sc ($J^p = 6^+$)	$2 \cdot 10^5$	107	335	10^{30}	9

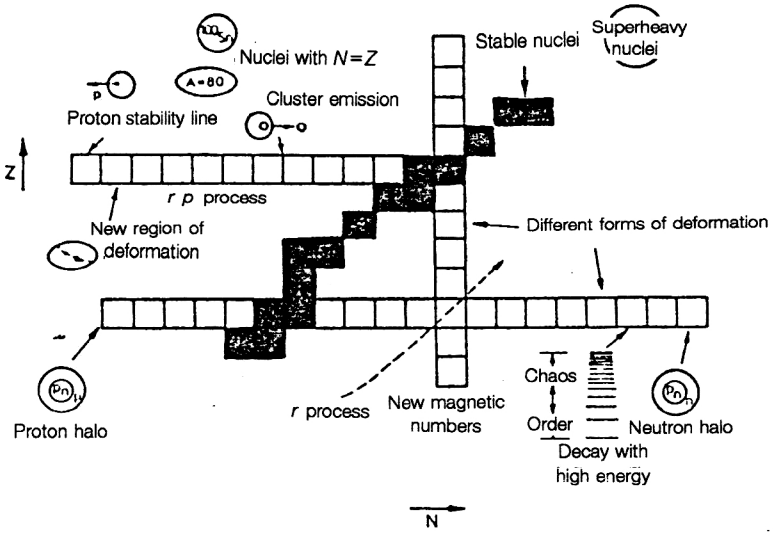

FIG. 20. Schematic representation of the $N-Z$ diagram of nuclides in regions of interest for investigation by means of radioactive beams.

and structures predicted earlier; 2) investigation of the mechanism of nuclear reactions, which will be strongly influenced by the structure of the interacting nuclei (study of pairing correlations in states analogous to Rydberg states and of collective interaction modes manifested in giant resonances and the use of variations of isovector type from the isospin); 3) finally, the investigation of rare processes (the formation of neutron-enriched compound nuclei, more exotic transfer reactions made possible by the lower Q value of the reaction for a neutron- or proton-enriched bombarding nucleus, and the production of compound nuclei with maximum angular momentum in symmetric reactions). Radioactive beams are used for investigations in astrophysics (production of exotic nuclei of interest for the study of r processes or s processes, measurement of the cross sections of nuclear reactions that take place in stars), and also in applied investigations. We shall now dwell on all the problems but will consider those for the solution of which the use of radioactive beams plays a fundamental role.

2.1. Investigation of nuclear structure by means of radioactive beams

The possibilities for investigating the structure of nuclei are determined by the intensity of the beams of radioactive isotopes that are to be investigated. Figure 20 shows schematically a chart of the nuclei and the regions of particular interest from the point of view of the investigation of exotic nuclear states. These nuclear states—new regions of deformations, new types of radioactivity, neutron and proton halos in nuclei, etc.—can be realized with high probability in experiments with radioactive beams, which make it possible to obtain nuclei in a wide range of N/Z, excitation energies, angular momenta, and deformations.

Binding energies and masses of nuclei

Predictions about the stability of the nuclei of light elements are directly related to the calculation of their masses. For the lightest nuclei, approaches to calculations of the masses based on various kinds of macroscopic models are of little use.

To calculate the masses of light nuclei, shell calculations and arguments that are based to some degree on the isotopic invariance of the nuclear forces are the most suitable. Isotopic invariance makes it possible to introduce the concept of isospin and regard nuclei with the same A as different states of the system of A nucleons.

In accordance with this, the total energy of the A nucleus can be represented as a sum of three terms: the nuclear part $E^A_{\text{nucl}}(T)$, which is due to the interaction between the nucleons and depends only on the isotopic spin, the energy $E^A_{\text{coul}}(Z)$ of the Coulomb interaction between the protons, and the masses of the neutrons and protons:

$$E^A_{\text{tot}}=E^A_{\text{coul}}(T)+E^A_{\text{coul}}(Z)+N_{MN}+Z_{MP}. \tag{19}$$

For the Coulomb energy of the nucleus, one usually takes the corresponding expression for a uniformly charged sphere with radius $R=r_0A^{1/3}$:

$$E^A_{\text{coul}}=\frac{3}{5}\frac{e^2Z(Z-1)}{r_0A^{1/3}}. \tag{20}$$

Exact calculation of the Coulomb energy is impossible, since, as a rule, the wave functions of the nuclear states are not known. Therefore, practical approaches to the calculation of nuclear masses are based to the maximum extent on empirical data on neighboring nuclei. One of the simplest of these is the three-term mass formula.[30]

Since the Z projection of the isotopic spin is not equal to $T=A/2-Z$, the Coulomb energy contains T_Z to a power not higher than the second, and the total energy of the nucleus can be represented as a polynomial of second degree in T_Z:

$$E^A_{\text{tot}}=a(T)+bT_Z+cT_Z^2. \tag{21}$$

This is a rather widely used form of the mass formula which can be applied to the same states of an isotopic multiplet and makes it possible to calculate nuclear masses if the coefficients a, b, and c are known from independent data.

The most widely used and successful method of calculating the masses of light nuclei is based on the use of the Garvey–Kelson relations,[31] which relate the data on the mass differences of a series of nuclei that differ in their T_Z values by unity. These relations have the form

$$\sum_{i=1}^{a} C_i M(N_i Z_i)=0, \quad |C_i|=1. \tag{22}$$

The expressions for $\alpha=6$ are most widely used:

$$M(N+2,Z-2)-M(N,Z)+M(N,Z-1)-M(N+1,Z-2)$$
$$+M(N+1,Z)-M(N+2,Z-1)=0, \tag{23}$$

$$M(N+2,Z)-M(N,Z-2)+M(N,Z-1)-M(N+1,Z)$$
$$+M(N+1,Z-2)-M(N+2,Z-1)=0. \tag{24}$$

Experience shows that the Garvey–Kelson method seldom predicts nuclei to be less stable than they actually are when calculations are made for the lightest nuclei with large neutron excess. Thus, ^{8}He,^{11}Li,^{19}C were found to be bound although the calculations predicted instability of these nuclei.

For predicting the stability of neutron-rich lightest nuclei, a purely empirical extrapolation of the dependence of the neutron binding energy on the number of protons at constant number of neutrons was found to be rather successful.

Although this extrapolation method does not have a rigorous foundation, it does appear to be suitable for predicting the masses of unstable nuclei. As the boundary of nuclear stability is approached, the neutron binding energy tends to zero, and it is obvious that pairing effects begin to play a role. This is confirmed by the behavior of the binding energies of the last nuclear-stable heavy isotopes of the light elements from helium to oxygen, for which nuclei with an even number of neutrons are stable. Thus, the nuclear potential for nuclides at the boundary of nuclear stability is not capable of confining single neutrons in a bound state, and only the additional *nn* interaction can give rise to nucleon stability of a nucleus. The analysis of pairing effects made by Migdal[32] proved the possibility of forming near the nuclear surface not only dineutrons but also cluster states of a larger number of correlated neutrons.[33] However, it is not only the pairing effects that are responsible for the dependence of the nuclear stability on its neutron excess $\eta=(N-Z)/A$. The averaged theoretical dependence of the nuclear energy determined by the symmetry energy is directly related to η. On this dependence there are superimposed even—odd effects and shell corrections, which are manifested in the specific experimental values of the binding energy. However, these effects are not universal. An example is provided by the so-called helium and hydrogen anomaly. The strongest growth in the stability of nuclei with increasing number of neutrons is observed for the ^{6}He–^{8}He pair of nuclei, for which it is greater than 1 MeV (see Fig. 21). If one examines the binding energies of the odd isotopes of helium, it is found that the transition from ^{5}He to ^{9}He i.e., the addition of four neutrons, hardly changes the energy of these nuclei. There is no microscopic explanation of the unusual stability of superheavy helium isotopes, and therefore the question arises of whether it is due to the fact that these nuclei have a neutron excess much greater than in ordinary nuclei. A similar anomalous raising of the stability with increasing neutron number is observed in the hydrogen isotopes (on the transition from ^{4}H to ^{4}H the stability also increases by almost 1 MeV (see Fig. 20), but here this occurs for the odd isotopes, and therefore

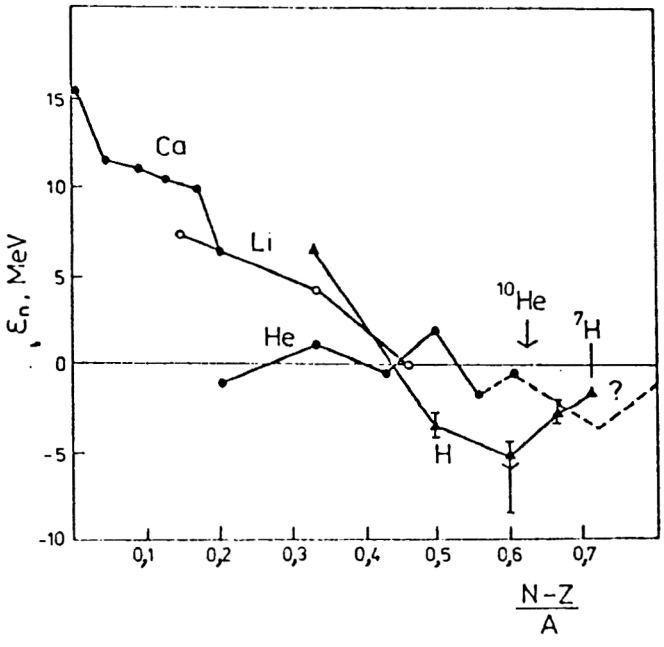

FIG. 21. Dependence of neutron binding energy on the relative neutron excess for isotopes of the lightest elements.

the explanation of this effect could be the influence of the centrifugal barrier (for neutrons with $l=0$) on the increase of the nuclear stability.[34] Estimates of the penetrability of the centrifugal barrier show that for $l=6$ and binding energy 0.5 MeV the lifetime can reach 10^{-16} s.

At the present time, it has been established experimentally that an increase in the number of neutrons leads to irregularity in the configuration of the shape of the isotopes. The equilibrium shape of the nucleus can be not only spherical but also nonspherical (deformed), and for some isotopes, especially near shells closed with respect to N, for which a compact spherical shape is assumed in the shell model, several equilibrium states can coexist. For example, use of the experimental values of the masses of a chain of neutron-rich isotopes of the odd element sodium ($Z=11$) in Ref. 35 showed (Fig. 22) that for the ^{30}Na isotope (which lacks one neutron to make up a closed shell with $N=20$) the potential energy includes not only the spherical equilibrium shape but also a minimum corresponding to a deformed state with quadrupole deformation parameter ~0.35. For the ^{31}Na isotope with closed $N=20$ shell, there are two equally probable spherical and deformed shapes. With increasing occupation by neutrons, a nonspherical shape with quadrupole deformation parameter of ~0.4 becomes the ground configuration of the nucleus (an example is ^{33}Na).

It is known that in a nonspherical nuclear potential there is lifting of the degeneracy of the levels with respect to the magnetic quantum number. Figure 23 shows the evolution of the splitting of the single-particle levels of the ^{35}Na nucleus with increasing value of the quadrupole deformation parameter; this was first investigated in Ref. 35. It can be seen that with increasing deformation the sublevels with smaller spin projections are "immersed" in a band of bound states (negative energy along the ordinate), whereas for components with

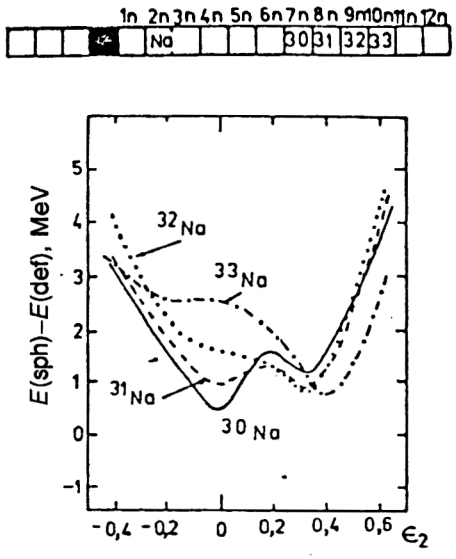

FIG. 22. Difference of potential energies (of spherical and deformed nuclei, ordinate) in the ground state for sodium isotopes as function of the deformation parameter ε_2 ($\varepsilon_2>0$ corresponds to elongation, $\varepsilon_2<0$ to flattening).[35]

large spin projections the opposite tendency is observed.

The development of appreciable static deformations in nuclei with anomalous N/Z can be the reason for the formation of a new region of nuclear shape isomers. In this case one can expect superheavy isotopes that are not nucleon stable in the spherical nuclear potential can become nuclear stable in the deformed state. As a consequence of this, the "ordinary" boundary of nuclear stability can be significantly shifted in the direction of a large neutron excess, and one cannot rule out the possibility of the formation of a new region of nuclear stability beyond the boundary of nuclear stability and having a number of neutrons corresponding to an appreciable excess of the critical N/Z value for the case of spherical nuclei.

A similar effect of deformation, giving rise to enhanced stability of nuclei, is also found for the heavy isotopes ^{24}O and ^{26}O (Ref. 36). It follows from all that we have said above that the experimental determination of the binding energies and masses of nuclei is one of the fundamental problems of nuclear physics. This problem is directly related to the problem of obtaining beams of radioactive nuclei. Using one of the methods described above—fragment separators or ISOL—one can obtain beams of radioactive nuclei far from the stability region and investigate their properties. Moreover, as was shown in the previous section, the fragmentation method makes it possible to produce and investigate nuclei near the boundaries of nucleon stability.

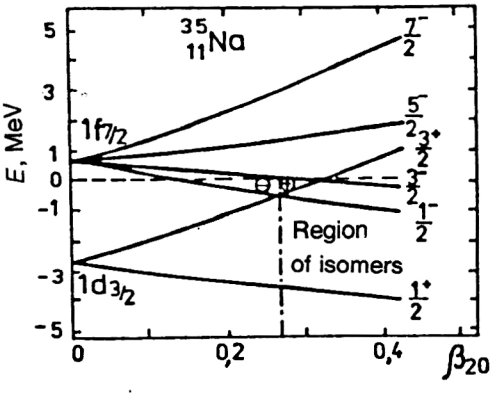

FIG. 23. Single-particle levels of neutrons (ordinate) in the ^{35}Na nucleus as function of the quadrupole deformation parameter β_2 made under the assumption of a deformed potential of Woods–Saxon form. A negative value of the energy eigenvalues (ordinate) corresponds to bound states of the ^{35}Na nucleus.

After beams of radioactive nuclei had been obtained, it became possible to measure accurately the masses of the nuclei ($\Delta M/M=10^{-4}$–10^{-6}). This is usually done by means of time-of-flight systems with sufficiently long flight base L (up to 2–3 km). In this case, the mass resolution is determined by

$$\frac{\Delta M}{M}=2\left[\frac{\Delta T}{T}+\frac{\Delta L}{L}\right]+\frac{\Delta E}{E}. \tag{25}$$

A large cycle of measurements of the masses of light nuclei was undertaken at the accelerator complex GANIL in France using the SPEG spectrometer with flight base 82 m and a beam of accelerated ^{48}Ca ions.[37] In these experiments, beams of radioactive nuclei from ^{27}F to ^{46}Cl were obtained and their masses determined.

The two-neutron binding energies (S_{2n}) in the nucleus obtained for these values of the nuclear masses are presented in Fig. 24. It can be seen that with increasing number of neutrons after the shell $N=20$ there is observed to be an appreciable increase in the stability of nuclei in the region of F, Ne, Na, and Mg. At the same time, the shell with $N=28$ plays a stabilizing role for nuclei of the isotopes of Si, P, S, or Cl. Such behavior of the neutron binding energy should be explained in the framework of various mass formulas. At the same GANIL accelerator, experiments have been begun on measurement of the masses of radioactive nuclei using a second cyclotron. Exotic nuclei produced as a result of interaction of a beam of ions accelerated in the first cyclotron with a target are accelerated in the second cyclotron. For the cyclotron, the conditions of acceleration depend on the magnetic field B, the acceleration frequency ω, the mass M of the accelerated particle, and its ionic charge and are determined by the ratio $B/\omega=q/M$. Under these conditions, detecting a nucleus at the exit from the cyclotron, one can determine its mass to an accuracy down to 10^{-5}–10^{-6}. Such a method can be extremely interesting and effective for determining the mass of nuclei with $Z>100$, and also for measuring the masses of the ground and isomer states of spontaneously fissioning isomers produced in complete fusion reactions at energies 5–10 MeV/A after the first cyclotron.

Neutron and proton halos in nuclei

Neutron-rich nuclei near the stability boundary have a comparatively low binding energy (we are referring here to nuclei stable with respect to neutron emission). Because of this, their sizes can be appreciably greater than that of ordinary nuclei. The low binding energy ε_n of the last neutron has the consequence that the wave function of the relative

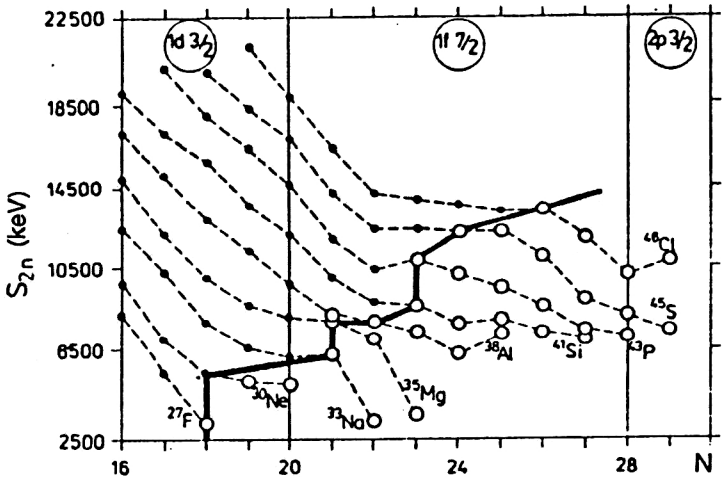

FIG. 24. Binding energy of two neutrons as function of the number of neutrons.[37] The heavy line is drawn through the last isotopes with known masses before the experiments described in Ref. 37. The open symbols represent new results.

motion of this neutron and the residual nucleus must have a very extended tail. For example, if the neutron is in the p state, then outside the interaction region the wave function has the form

$$R_n(r)=\left(1+\frac{1}{V_n r}\right)e^{-x_n r}, \quad x_n=\sqrt{\frac{2\mu\varepsilon_n}{\hbar^2}}. \tag{26}$$

At $\varepsilon_n=1$ MeV (assuming $\mu=1$), the tail of the neutron wave function extends over a distance ~ 5 fm, for $\varepsilon_n=0.1$ MeV over 15 fm. It is obvious that the radius of such a nucleus can differ strongly from the value $R=r_0A^{1/3}$.

In the region of light nuclei, the largest ratio of the numbers of neutrons and protons has now been achieved. Whereas for the intermediate and heavy regions of nuclear masses this ratio $X=(N-Z)/A$ lies in the range 0.1–0.2, for light nuclei it is 0.45 (^{11}Li) to 0.55 (^{9}He). The strong enrichment of nuclei with neutrons significantly changes the distribution of the neutron and proton densities p_n and p_p in the nuclei (see Fig. 25), which at the present time can be determined only from experiments with radioactive beams. For such strongly neutron-enriched nuclei there has been found to exist a "neutron halo," which influences the structure and properties of these nuclei.

The existence of nuclei with halos was discovered in a measurement of the interaction cross sections of these nuclei. It was found that the nuclei ^{11}Li,^{17}B,^{14}Be have relatively large interaction cross section (Fig. 26). This can be explained by the existence in them of halos of weakly bound neutrons. The interest in such nuclei arises for various reasons, above all their unusual properties.

In strongly neutron-deficient nuclei that lie at the boundary of nucleon stability and have a low binding energy of a proton (or pair of protons) one can observe an unusual distribution of the electric charge—an extended surface layer enriched with protons. This can lead to the appearance of a proton halo in such nuclei analogous to the well-known neutron halo in the ^{11}Li nucleus. However, the conditions for the existence of a proton halo are less favorable than for a neutron halo. A proton halo is hindered by the Coulomb forces of repulsion between the outer protons and the core; these forces decrease with the distance much less slowly than the nuclear forces. Because of this, protons cannot be kept at an appreciable distance from the core. Therefore, instead of a proton halo there can be a comparatively thin (~ 0.5 fm) surface layer enriched with protons (see Fig. 27).

The existence of a proton halo or proton surface layer is expected in nuclei containing several protons above a doubly magic core. Examples of such nuclei are:

^{19}Na (3 protons above ^{16}O–$8p+8n$)
^{20}Mg (4 protons above ^{16}O)
^{42}Ti (2 protons above ^{40}Ca–$20p+20n$)
^{43}V (3 protons above ^{40}Ca).

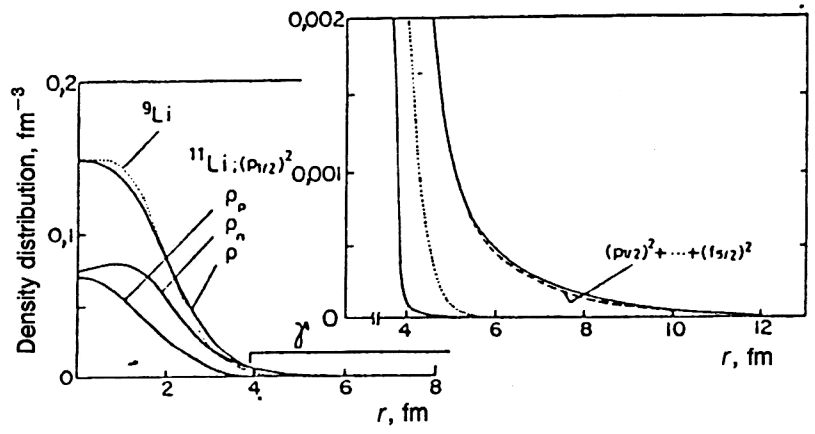

FIG. 25. Distribution of the density of neutrons and protons in the ^{11}Li nucleus.[38]

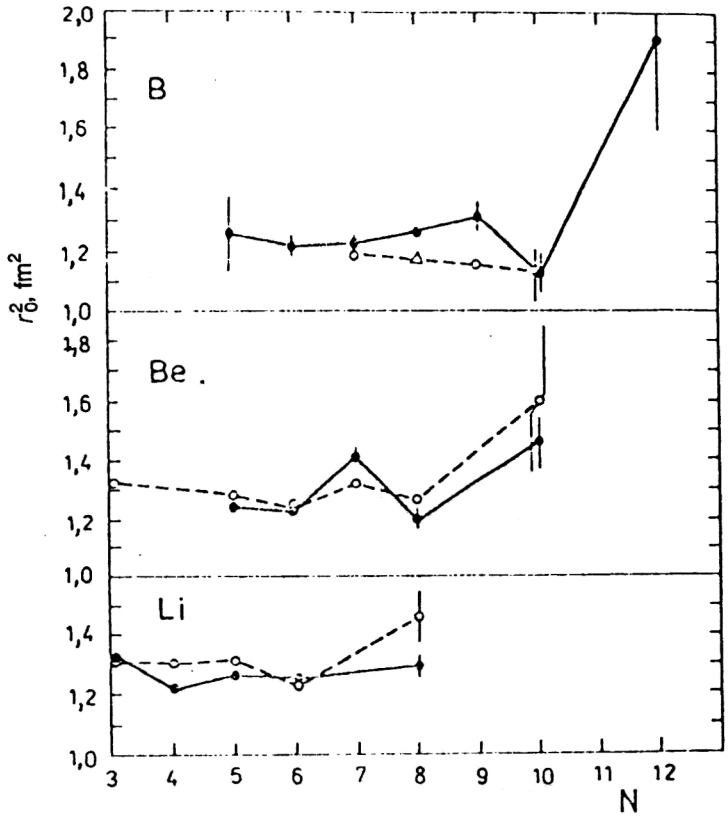

FIG. 26. Dependence of mean square interaction range of nuclei of different isotopes of Li, Be, and B as obtained in Ref. 39 (dashed line) and Ref. 40 (solid continuous line).

These nuclei can be obtained in reactions with heavy ions, for example, $^{12}C(^{14}N,4n)^{19}Na$, $^{27}Al(^{20}Ne p4n)^{42}Ti$.

The distribution of the electric charge in these nuclei can be measured in experiments using the method of laser spectroscopy.

An indication of a proton halo was obtained in an investigation of the neutron-deficient isotope ^8B, which has a proton binding energy 0.14 MeV (Ref. 41). This nucleus has an anomalously large electric quadrupole moment $Q=68.3$ mb, whereas in accordance with the shell model it must be only 24.9 mb, i.e., smaller by a factor 3. From the value of Q we obtain the charge radius $\langle r^2\rangle_p^{1/2}=2.98$ fm, which can be compared with the radius for the neutron core: $\langle r^2\rangle_n=2.20$ fm.

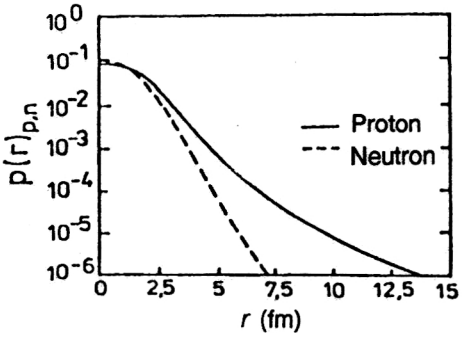

FIG. 27. Density distribution of neutrons and protons in the ^8Be nucleus.[41]

Investigation of resonances in exotic nuclei

Exotic nuclei open up unique possibilities for investigating the effect of the various forces in stable nuclei. Indeed, the excitation energy of a monopole resonance is related to the nuclear compressibility by the simple equation

$$E_{GMR}=\hbar(K_A/m\langle r^2\rangle)^{1/2}. \tag{27}$$

The nuclear compressibility K_A can be described by the compressibility of infinite symmetric nuclear matter, K_∞, and surface compressibility K_s with correction K_c for charge asymmetry:

$$K_A=K_\infty+K_sA^{-1/3}+K_c\left(\frac{N-Z}{A}\right)^2+K_cZ^2A^{1/3}, \tag{28}$$

where K_s, K_∞, and K_c are the surface, isospin, and Coulomb coefficients. The value $K_\infty=-(250\pm25)$ MeV is well determined from experimental data on the giant monopole resonance. The value $K_c=-(320\pm180)$ MeV has a large error and was determined only from data on nuclei far from the stability line. In addition, parabolic dependence of K_c on $N-Z$ has not been proved. Measurements of the monopole resonance in exotic nuclei can solve the problem of determining K_c and prove a parabolic dependence on $N-Z$. This is very important not only for nuclear physics but also for astrophysics, where the compression of neutron-enriched matter determines the conditions of supernova explosions.

Dipole resonances associated with vibrations of the core of the nucleus with respect to the neutron halo are of great interest. For example, in the case of ^{11}Li the core, which consists of three protons and six neutrons, can execute vibra-

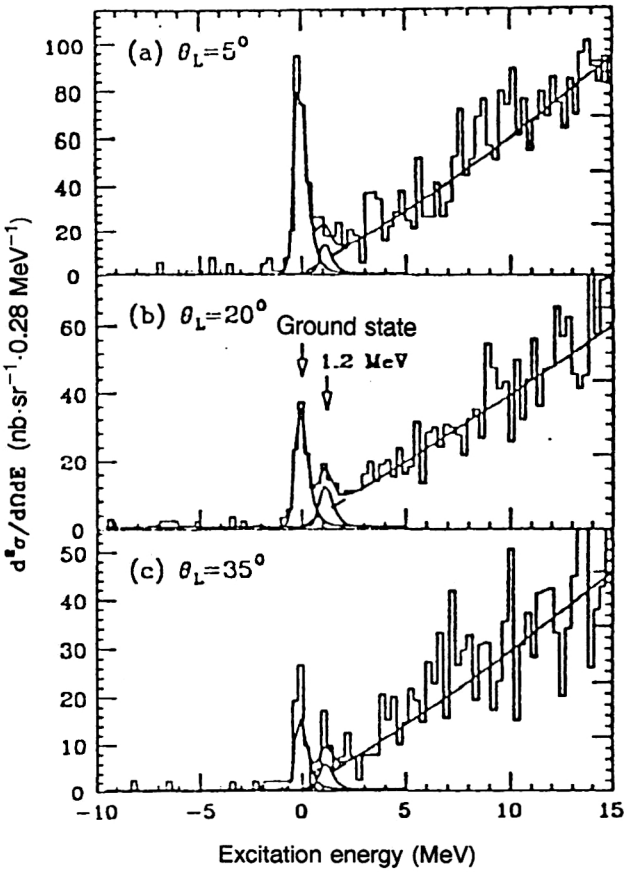

FIG. 28. Energy spectrum of π^+ in the reaction $^{11}B(\pi^-,\pi^+)^{11}Li$ (T_π=164 MeV) at three detection angles. The solid curve gives the calculated values of the three-body phase space. The peak with energy 1.2 MeV is ascribed to a soft mode of the dipole resonance.[42]

tions with respect to a halo of two neutrons. In Ref. 42 there was found to be a soft mode of a long resonance for the nucleus ^{11}Li in the $^{11}B(\pi^-,\pi^+)^{11}Li$ reaction (Fig. 28).

It was shown in this study that the energy $h\omega$ of such vibrations is related to the energy of the dipole resonance by

$$h\omega=\left|\frac{Z(N-N_c)}{N(Z+N_c)}\right|^{1/2} h\omega_{GDR}. \tag{29}$$

For nuclei strongly enriched with neutrons, $h\omega=(1/\sqrt{2})h\omega_{GDR}$. These resonances can be observed in direct reactions. For example, for the investigation of the giant dipole resonance in ^{11}Li the $^{14}C(^{11}B,^{14}O)^{11}Li$ reaction was used to measure the energy spectrum of ^{14}O and seek in it on the background of the curve corresponding to the phase space the resonance associated with vibration of the core relative to the halo.[43] In nuclei strongly enriched with neutrons there are predicted to be new types of collective vibrations at high excitation energy. Investigation of their microscopic structure may give information about the coupling of the isospin to these modes. On the other hand, the energy of the giant dipole resonance is not sensitive to the isospin and is determined by the expression

$$E_{GDR}=E_0+\alpha(N-Z)+b(N-Z)^2. \tag{30}$$

Therefore, measuring E_{GDR} for different neutron—proton ratios in a nucleus, one can obtain the dependence of the nuclear forces on the isospin.

Decays of exotic nuclei

The production of fairly intense beams of radioactive nuclei far from the stability boundaries opens up new possibilities for observing exotic decays, including delayed decays. For these nuclei, the difference between the masses of neighboring isotopes (the β-decay energy) can reach 20–30 MeV, and after β decay levels with high excitation energy can be occupied, this leading to the appearance of a broad energy region for different types of decay: β-delayed two-neutron and three-neutron decay and emission of tritons, α particles, and heavier particles.[34] Interesting from this point of view are the isotopes ^{11}Li and ^{8}He, which have a high value of the β-decay energy. For the ^{11}Li isotope, Q_β=20.7 MeV, and this makes all the types of decay listed above energetically allowed. Thus, the emission of a β-delayed triton for this nucleus is energetically favored and has a threshold 15.72 MeV for decay of ^{11}Li into ^{8}Li+t. The ^{11}Li decay scheme is shown in Fig. 29. This new type of decay was predicted for light nuclei far from the β-stability line in Ref. 44 and was observed experimentally in Ref. 45.

Delayed emission of tritium nuclei after β decay of ^{8}He has been observed experimentally.[45] The β-decay energy for this nucleus is Q_β=10.653 MeV and the thresholds for breakup of ^{8}Li into $\alpha+t+n$ and ^{5}He+t are 4.50 and 5.39 MeV, respectively. Both branches of decay occurring after β decay of the ^{8}He nucleus to the lithium level with energy 8.8 MeV and width Γ=1 MeV were identified.

The processes accompanying β-decay of neutron-rich nuclei were considered in detail in Ref. 46. Their theoretical description is based on calculation of the β-decay strength function $S_\beta(E)$, which determines, in terms of an integral with the Fermi function, the occupation of the levels of the daughter nucleus in β decay. The function $S_\beta(E)$ has a complicated structure of resonance type based on isobaric states (Fig. 30). The most important role is played by the tails of the Gamow—Teller resonance and states of the type of core polarization determined by proton—neutron-hole configurations and associated with a flip of the total angular momentum. These last are usually situated in the β-decay window.

The possibility of a (β^-,kn) process (k=1,2,...) is determined by the condition $Q_\beta>B_{kn}$, where B_{kn} is the energy of separation of k neutrons in the daughter nucleus (see Fig. 29). The analysis made in Ref. 46 shows that the region of nuclei that undergo delayed decay with emission of two neutrons has approached rather close to the boundary of the already identified nuclei. For some of the discovered nuclei, one can make a prediction of the probability of three-neutron and four-neutron decay.

The probability of emission of k neutrons is determined by

$$P_{kn}=\int_{B_{kn}}^{Q_\beta}\int_0^{Q_{kn}} I_\beta(U)W_n(U,E)dUdE, \tag{31}$$

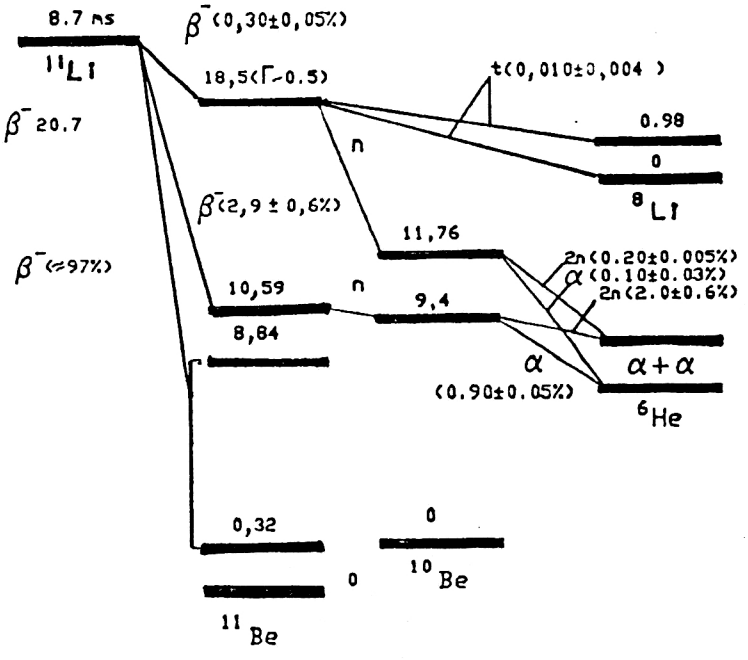

FIG. 29. Decay scheme of the ^{11}Li nucleus.

where $I_\beta(U)$ is the probability of occupation of the isobaric state in the daughter nucleus, and $Q_{kn}=Q_\beta-B_{kn}$. The inner integral over U gives the spectrum of the emitted neutrons, which is determined by their emission probability $W_n(U,E)$, which can be calculated in accordance with a statistical theory.

For rough estimates, one can use the expression

$$P_{kn}\approx 125(Q_{kn}/Q_\beta)^{4.35}[\%], \quad k\geqslant 2. \tag{32}$$

This does not take into account even—odd effects, which for $k\geqslant 2$ are already unimportant.

The most complete investigation of multineutron β-delayed emission was made for the Na isotopes. A review of experimental data and comparison with calculations was made in Ref. 35.

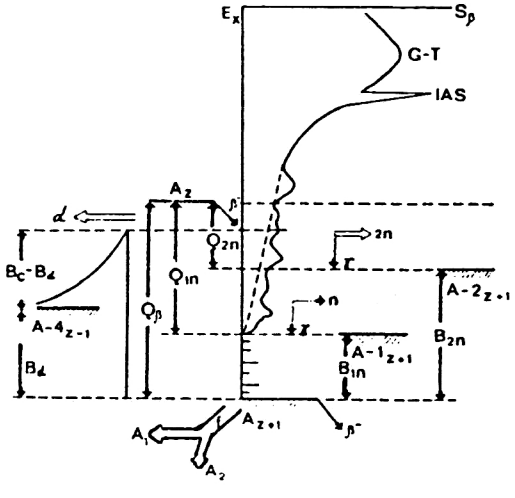

FIG. 30. Schematic representation of the process of β^+ decay.[46]

One of the most important questions is associated with the possibility of the emission of a correlated pair of two neutrons (a dineutron). In β-delayed decays, such a process has not been observed. The results of the calculations made in Ref. 46 predict a probability P_{2n} of dineutron emission several orders of magnitude less than the probability P_{n+n} of the cascade mechanism (for nuclei in the region ^{30}Na–^{55}K). These calculations are purely statistical and do not take into account the possibility of correlation of neutrons on the surface, which may enhance the process. The search for delayed dineutron emission is today evidently one of the most realistic routes to understanding the nature of such decays in heavier nuclei. To solve the problem of the mechanism of two-neutron and multineutron decay, it is necessary to make an experimental investigation of nuclei that undergo delayed neutron decay. Figure 31 gives the results of measurements of the neutron multiplicity after β decay of ^{17}B nuclei taken from Ref. 47. It can be seen that with a relatively high probability emission of two, three, and four neutrons takes place from this nucleus. An important experimental problem is the investigation of the correlations of these neutrons and the possibility of emission of entire neutron systems consisting, for example, of four neutrons (tetraneutron). Such experiments are currently being made using beams of radioactive nuclei.[48]

Recently interesting effects associated with observation of proton decay of neutron-deficient nuclei from the ground state were found, namely, the existence of an increased lifetime with respect to proton decay for nuclei with mass $A=110$ and 150 and also two-proton radioactivity from the ground state. Further investigation of these effects, which directly give important information about the influence of shell effects, angular momenta, and deformation on the decay of exotic nuclei, can be continued only in fusion reactions with radioactive beams. For example, in the SPIRAL

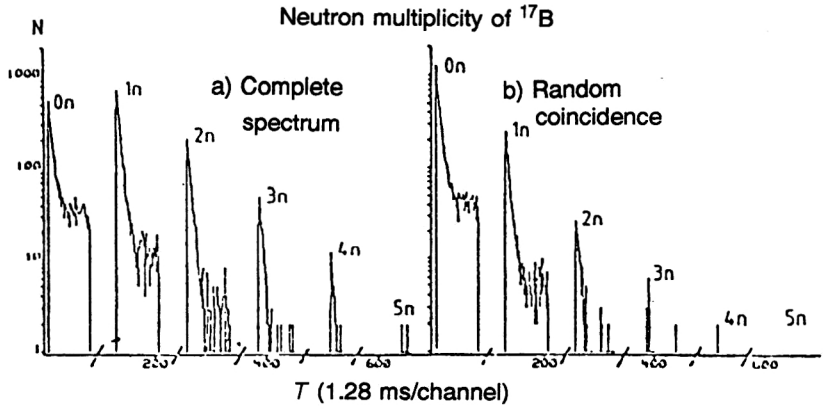

FIG. 31. Experimentally measured multiplicity of neutrons[47] after β decay of ^{17}B.

project (France) it is proposed to obtain nuclei such as ^{87,89,90}Pd, ^{97,98}Sn, ^{132}Gd, and ^{138}Dy which undergo $2p$ decay in reactions of the type

^{64}Zn(^{74}Kr,$2p4n$)^{132}Gd (σ=760 ml, E_{beam}=380 MeV),

^{64}Zn(^{74}Kr,$2p3n$)^{132}Gd (σ=6.3 ml, E_{beam}=350 MeV).

It is proposed to use such reactions to investigate the cluster emission of neutron-deficient nuclei.

An interesting proposal for investigating proton radioactivity from a high-spin isomer state was made in Ref. 49, in which it was proposed to measure the characteristics of proton decay near the $g_{9/2}$ shell in isotopes with $N=Z$ (^{95,97}In[25/2+], ^{96}Cd[16+], ^{95}Cd[23/2+], ^{95}Ag(23/2+]). In this case, the emission of a proton will be determined by the changes of the angular momentum and the microscopic factor, which for the considered nuclei lead to an increase in the probability of proton emission.

2.2. Nuclear reactions with beams of radioactive nuclei

Elastic scattering of beams of radioactive nuclei

As is well known, experiments on the elastic scattering of nuclei give information on the shape and magnitude of the nuclear potential, and also on the parameters of the nuclei themselves, namely, their structure, mean square radii of the distributions of the nucleons, charges, etc. As a rule, various approaches to the analysis of the angular distributions of elastically scattered nuclei are used—the semiclassical approach[50] and a phenomenological or semimicroscopic optical model.[51] In accordance with the semiclassical treatment of elastic scattering, a particle moves along a Coulomb trajectory and can undergo inelastic interaction, which removes it from the elastic channel. In this case, investigating the dependences of the experimental elastic-scattering data on the distance of closest approach $D=(a/2)$ $(1+\cos\theta/2)$, where $a=Z_pZ_te^2/E$ (Z_p and Z_t are the charges of the projectile nucleus and the target nucleus, E is the energy of the bombarding nucleus in the center-of-mass system, and θ is the c.m.s. scattering angle), one can determine both the interaction range of the particles and the radius of strong absorption, i.e., the distance between the centers of the colliding nuclei at which the intensity of the flux in the elastic channel is reduced by a half. In Ref. 52, beams of the radioactive nuclei ^{6}He and ^{9}Li were obtained and their elastic scattering by lead was investigated.

Figure 32 shows the dependence of the ratio of the differential cross section of elastic scattering of the nuclei ^{6}He and ^{6}Li to the differential cross section of Rutherford scattering of these nuclei as a function of the distance of closest approach $d=D/(A_T^{1/3}+A_p^{1/3})$. Note the strong difference between these dependences for the case of ^{9}Li and for the two other nuclei. For further analysis of this difference, the optical model was used in conjunction with the real component of the folding potential. It was concluded that there is significant transparency of the peripheral interaction region of the investigated elastic channel (in the given case, scattering of ^{9}Li by ^{208}Pb). This transparency is not achieved by a weakening of the probability of peripheral reactions (i.e., of the imaginary component of the optical potential of ^{9}Li compared with ^{7}Li) but as a result of a significant enhancement of the real component of the nucleus–nucleus interactions at large distances between the centers of mass of the ions. It

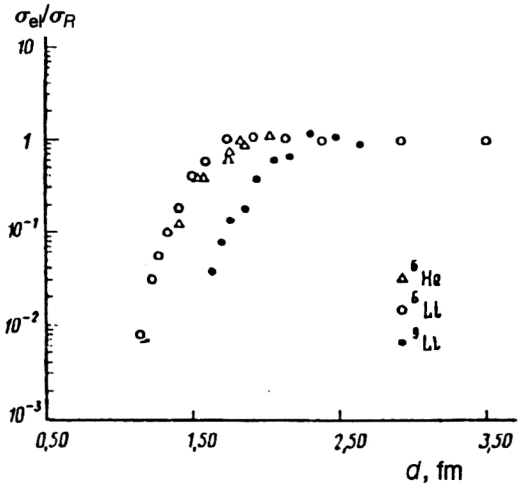

FIG. 32. Dependence of the ratio of the cross section for elastic scattering of the ^{6}He, ^{6}Li, and ^{9}Li nuclei to the Rutherford cross section on a lead target on the parameter of closest approach d of the two nuclei.[52]

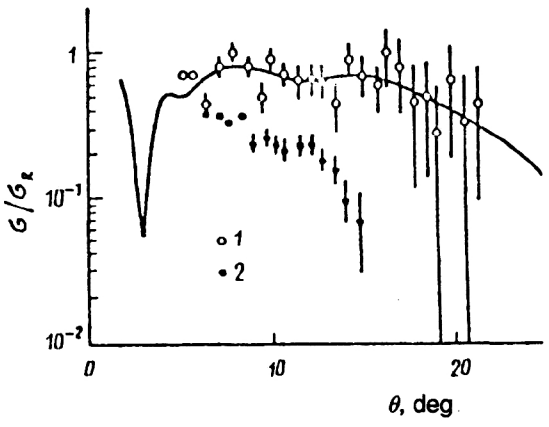

FIG. 33. Angle dependence of ratio of cross sections for elastic scattering of ^{11}Li (*1*) and ^{7}Li (*2*) on a silicon target to the Rutherford cross section.[54]

was concluded in Ref. 53 that this effect has a dynamical nature, namely, there is dynamic polarization of the incident particle. Joint Dubna–GANIL experiments on elastic scattering of ^{11}Li (25.4 MeV/nucleon) by ^{28}Si nuclei showed[54] that the angular distributions of elastically scattered ^{7}Li and ^{11}Li nuclei differ strongly (Fig. 33). In the case of ^{11}Li scattering, in contrast to the case of ^{7}Li, there was no sharp decrease in the scattering cross section as a function of the angle. In an analysis of data on the optical model, this leads to the necessity of introducing a strongly increased diffuseness parameter of the real part of the potential; in principle, this can be explained by the presence of a neutron halo in this nucleus. Such behavior of the angular distribution of ^{11}Li elastic scattering can also be explained by a manifestation of rainbow scattering at angles greater than 10° in the center-of-mass system.

Rainbow scattering of light radioactive nuclei

Beams of radioactive nuclei make it possible to pose new physics problems that previously could not be undertaken. One of them is the question of the isospin dependence of the nucleus–nucleus potential. In general form, the optical potential of nuclei a and A can be represented in the form of two parts, one of which is determined solely by the masses of the colliding nuclei, while the second depends on their neutron or proton excesses (projections of the isotopic spins):

$$U(a,A)=U_0(a,A)+U_T(a,A). \tag{33}$$

It is natural to expect the occurrence of an isospin-dependent term in the potential for nuclei in which the excess of nucleons of one species strongly changes the complete structure of the nucleus. The potential may depend on the projections of the isospin of the colliding nuclei, since in a nuclear medium with $N\neq Z$ a neutron and proton interact differently. This effect is a consequence of the existence of a symmetry energy and is manifested in nucleon–nucleus collisions. Therefore, for the nuclei a and A (both with $N\neq Z$), one can expect the appearance in the potential of a term that depends on their isospins.

There are almost no direct data on the isospin part of the potential. Therefore, estimates are made by extrapolating the data on the nucleon–nucleus potential to more complicated systems.

The nucleon–nucleus potential is usually written in the form

$$V=V_c f_0(r)+\frac{1}{2}\,t_z\,\frac{N-Z}{A}\,V_1 f_1(r)\approx\left[V_0+\frac{V_1}{A}\,t_z T_z\right]f(r), \tag{34}$$

where $t_z=+1/2$ for neutrons and $-1/2$ for protons, and the radial dependences are taken to be the same. From estimates based on the symmetry energy, the value obtained for V_1 is $\sim$100 MeV, while experimentally it is 70–120 MeV.

It was proposed in Ref. 55 to obtain data on the isospin part of the nucleon–nucleus potential from experiments on rainbow scattering of radioactive nuclei. A fairly large number of experimental and theoretical studies has recently been devoted to the investigation of this effect. This is explained by the possibility of obtaining important information on the properties of two interacting nuclei–their nuclear potentials, structure, etc. By analogy with the laws of optics, there can be diffraction of waves corresponding to incident and absorbed particles. In this case, the angular distribution of the scattered nuclei is broader than in the case of ordinary elastic scattering and is extremely sensitive to the surface properties of the two interacting nuclei. It is assumed in Ref. 56 that these experiments will make possible the following advances:

1) a significant decrease in the arbitrariness in the choice of the potential;

2) study of the radial dependences $f(r)$, since the rainbow effect is related to the origin of the particles in the depth of the nucleus;

3) observation of a qualitative result—displacements of the rainbow maximum in the angular distributions of the scattering due to the different depths of the potential.

In this study an attempt is made to estimate the magnitudes of the shift for the case of the scattering of two nuclei with different T_z by the same target nucleus. The position of the angle of the nuclear rainbow for a potential of Woods–Saxon type is[57]

$$\Theta_{NR}\cong 0.56\,\frac{V}{E}\left(\frac{R}{a}\right)^{1/2}, \tag{35}$$

where E is the energy of the particles, and V, R, and a are the parameters of the real part of the potential.

Extrapolating the expression (2) to the nucleus–nucleus potential, we obtain

$$\Delta\Theta_{NR}\cong 0.56\,\frac{V_1}{AE}\left(\frac{R}{a}\right)^{1/2} T_z\Delta T_z. \tag{36}$$

As a rule, the observed shift will be somewhat less because of the Coulomb repulsion.

Thus, investigation of the scattering of nuclear isobars in the region of the nuclear rainbow makes it possible in principle to determine the isospin part of the potential, but it does require very accurate measurements. The main requirements on such measurements are the following:

1) The energy of the incident particles must be such that the nuclear rainbow is manifested well in the angular distributions. The lower limit is 15–20 MeV/nucleon, and the upper limit, at which the rainbow maximum is still outside the region of the diffraction oscillations, is ~300 MeV/nucleon. High energies have a further advantage: At them, the nuclear transparency is maximal. At such energies, nuclear rainbow effects are expected at angles 10°, and the measurements require angular resolution ~0.1°–0.3°.

2) To obtain the greatest shift $\Delta\theta_{NR}$ of the rainbow maxima, the target nucleus must have the largest possible T_z. However, heavy nuclei are evidently unsuitable, since the nuclear rainbow effect has not been found for them (see, for example, Ref. 58, in which measurements of $^{12}C+^{208}Pb$ scattering at $E_{lab}=200$ MeV/nucleon were made).

3) The difference ΔT_z of the incident nuclei must be maximal. Restrictions on the choice of the pairs of scattered nuclei are imposed, first, by the possibility of obtaining them in sufficient number and, second, by the condition that their lifetime be comparable with the acceleration times. In addition, they must be sufficiently light ($A\approx 20$), since the heaviest incident nucleus for which the nuclear rainbow phenomenon has been observed is currently ^{16}O (Ref. 59). It is possible that with an increase of the energy to 100–300 MeV/nucleon it will be possible to advance to heavier nuclei.

We give below the expected values of the angles of displacement of the rainbow maximum for the scattering of a pair of nuclei with $\Delta T_z=2$ by three target nuclei: ^{14}C,^{48}Ca,^{96}Zr. It can be seen that the shift is $\Delta\theta\geqslant 1°$. Bearing in mind the features of the expected angular distributions, this value is accessible to measurement in experiments with radioactive beams.

The shifts of the rainbow maxima for the scattering of nuclei with $\Delta T_z=2$ ($A=11$, $E=85$ MeV/nucleon) are:

Target nucleus	$\Delta\Theta$, deg
^{14}C	1.6
^{48}Ca	2.1
^{96}Zr	2.3

To estimate the expected effect, we can use data on $^{12}C+^{12}C$ scattering[60] obtained at the Hahn–Meitner Institute (Berlin) using VICKSI at energy 240 MeV. Figure 34 shows the calculated[60] cross section together with the experimental data. It can be seen that at angles $\theta_{cms}>40°$ there is an increase of the cross section, which can be explained by rainbow scattering.

Thus, study of rainbow scattering with beams of radioactive nuclei can give information about the isospin part of the nucleus–nucleus potential. The role of this component of the potential in the interaction of nuclei, about which there are currently practically no data, increases in importance with increasing distance of the nuclei from the stability boundaries. The requirements of the parameters of radioactive beams are rather high, and will apparently be realized in the accelerator systems of the new generation—heavy-ion storage rings.

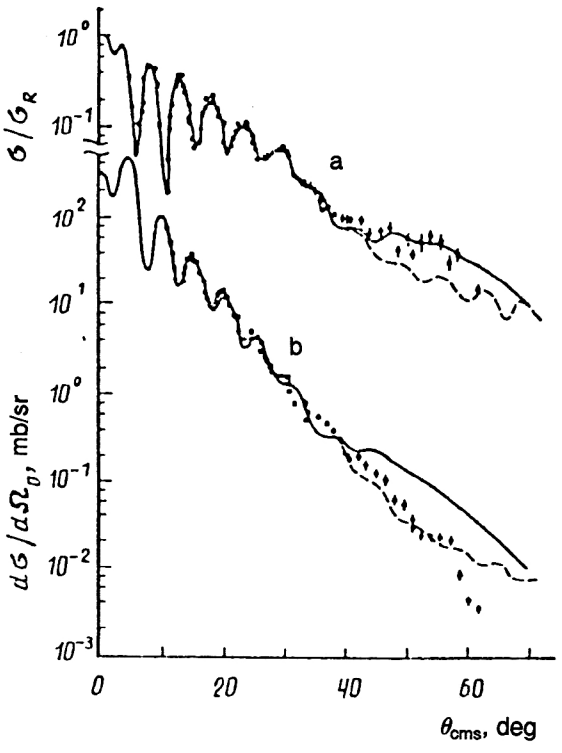

FIG. 34. Dependence of the cross section for elastic (a) and inelastic (b) ($E^*=4.44$ MeV) scattering on a carbon target at $E(^{13}C)=20$ MeV/A. The dashed curve gives the results of Ref. 60.

Rearrangement reactions

To this class of reactions there belong processes associated with exchange between the target nuclei and the bombarding particle of several nucleons without significant change of the excitation energy. Charge-exchange reactions can also be included among such reactions. They possess a number of characteristic features compared with transfer reactions. Rearrangement reactions are successfully used to obtain information about strongly neutron-enriched nuclei of light elements (superheavy isotopes of hydrogen, helium, and lithium). In this case, one uses bombarding ions ^{7}Li,^{9}Be,^{11}B,^{14}C,^{18}O at energies up to 30 MeV/A and measures the energy spectra of the nuclei complementary to the investigated nucleus. For example, in the case of the $^{14}C(^{9}Be,^{14}O)^{9}He$ reaction, investigating the energy spectrum of ^{14}O, it is possible to obtain information about the structure of the ^{9}He nucleus and its binding energy.[34] The cross section of such reactions depends on the Q value. The possibilities of using this method are also restricted by the requirement of having a known nucleon—stable nucleus complementary to the investigated one. From this point of view, the possibilities for these investigations are extended by using beams of radioactive nuclei. For example, to obtain information about the stability of ^{7}H nuclei one can use the reaction ($^{8}He(d,^{3}He)^{7}H$) with ^{8}He beam on a deuterium target for ^{10}He nuclei, one can use the reaction $^{8}He(t,p)^{10}He$, etc. To reduce the background in the experiment in this case, it is necessary to measure coincidence between the complementary particle (in the given case ^{3}He or p) and the decay

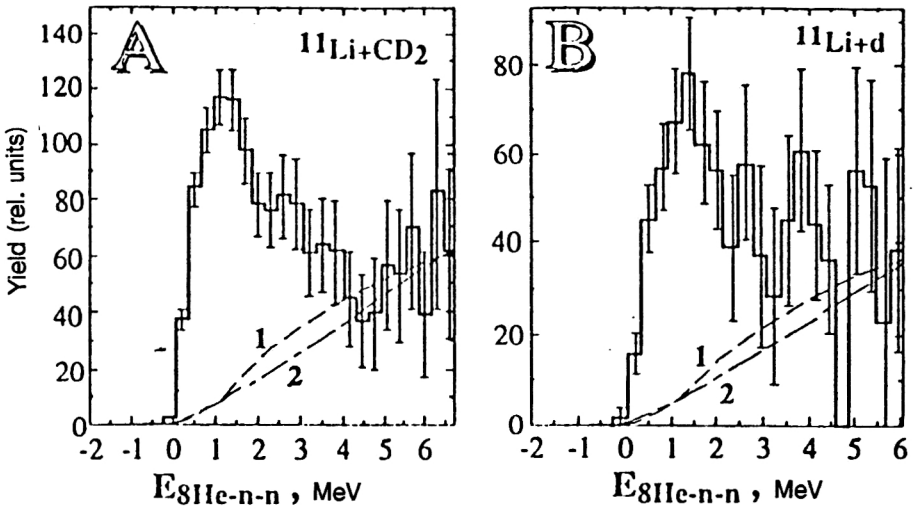

FIG. 35. Invariant ^{8}He$+n+n$ mass spectrum for the CD$_2$(^{11}Li,$2n$,^{8}He) reaction.[61] The spectrum (B) is obtained by subtraction from spectrum (A) measured on the carbon target. The dashed curves *1* and *2* are calculated for the ^{8}He$+n$ and ^{8}He$+n+n$ phase spaces, respectively.

product of the investigated particle (^{3}H in the first case and ^{8}He in the second). These experiments are extremely important for investigating the properties of neutron matter and also for solving problems in astrophysics.

The use of light targets (hydrogen, deuterium, helium, tritium) is of great interest for investigation of the structure of exotic nuclei and the mechanism of nuclear reactions with radioactive beams. In this case, the conditions of the experiment are considerably eased in the case of the so-called inverse kinematics, since because of the large translational velocity the angular distribution of the products becomes narrow, and it is not necessary to use 4π-detecting systems; in addition, the recoil nuclei (in the given case, the light nuclei) have a fairly narrow angular distribution with a maximum at a large angle, and this facilitates detection of these nuclei. Reactions in inverse kinematics with radioactive beams have been recently used to investigate the structure of ultra-neutron-rich isotopes of the lightest elements. In the study of Ref. 61 a measurement was made of resonances in the ^{10}He nucleus using inverse kinematics. The CD$_2$ (^{11}Li, $2n$^{8}He) reaction was investigated at the accelerator complex RIKEN (Japan) by means of a radioactive beam of ^{11}Li with intensity $2\cdot10^4$ particles/s and energy 61 MeV/nucleon. For unambiguous identification of the reaction channel, coincidences of ^{8}He with neutrons were measured. Figure 35 gives the spectrum of invariant masses for this reaction. The authors of the study identified the peak in this reaction as the ground state of a resonance in the ^{10}He nucleus with energy 1.2 ± 0.3 MeV and width $\Gamma\leqslant1.2$ MeV. This is the first result of the use of radioactive beams to investigate the structure and resonances in the ultra-neutron-rich isotopes of the lightest elements. It is be hoped that inverse reactions of the type ^{8}He$+^3$H, leading to the nuclei ^{10}He$+p$, ^{6}He$+^5$H,^{4}He$+^7$H,^{3}He$+^8$H,^{9}Li$+^2n$,^{7}Li$+^4n$, etc., will make it possible to obtain spectroscopic information about these nuclei.

Proposals for experiments to investigate elastic scattering of radioactive nuclei by light targets (in inverse kinematics) have also been recently discussed.

In this case, the kinematics of the process is determined by simple relations that connect the angles in the laboratory system to those in the center-of-mass system:

$$\tan(\Theta_{\text{lab1}})=\frac{\sin\Theta_{\text{cms}}}{\frac{m_1}{m_2}+\cos\Theta_{\text{cms}}}, \tag{37}$$

$$(\Theta_{\text{lab2}})=\frac{\pi-\Theta_{\text{cms}}}{2} \tag{38}$$

(Θ_{lab1} is the scattering angle of the incident particle, and Θ_{lab2} is the scattering angle of the recoil nucleus).

Figure 36 shows the dependence of the scattering angles for the proton and ^{6}He in the case of bombardment of a hydrogen target by ^{6}He radioactive beams. The proton is detected in this arrangement of the experiment. The maximum deflection angle of the ^{6}He in this reaction does not exceed 10° in the laboratory system. One of the methodological problems in such an arrangement of the experiments is the need to have good angular resolution of the detector, which detects protons at large angles relative to the initial

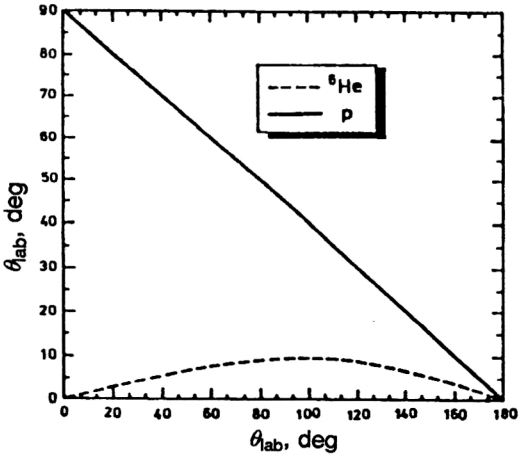

FIG. 36. Dependence of the ^{6}He scattering angles (dashed curve) on the proton scattering angle for the ^{6}He$+p$ reaction at 56 MeV of the ^{6}He.

beam. If a gas hydrogen target is used, this becomes problematic. This problem can be solved by using a so-called time-projection chamber,[62] which is a combination of a drift chamber with coordinate-sensitive proportional gaps. The gas volume of the chamber can itself be the target, and this makes it possible to detect with sufficient accuracy not only the energy of each particle that has interacted but also its scattering angle, i.e., to determine simultaneously all the kinematic characteristics of the particles that participate in the nuclear reaction.

Coulomb excitation of levels of rotational bands in odd–odd deformed nuclei

The Coulomb excitation of nuclei makes it possible to obtain important information about nuclear properties: the spectrum of collective levels, moments of inertia, quadrupole moments, deformation parameters, etc. Only stable nuclei have been well investigated and there are no data at all about unstable nuclei, since there are great difficulties in making targets out of them.

The use of beams of radioactive nuclei with energy 3–5 MeV/nucleon makes it possible to carry out successful measurements, since the cross sections of Coulomb excitation for deformed nuclei reach tens of barns in the region of light and intermediate deformed nuclei—the isotopes of Na, Al, Sc, Br, Rb. In these nuclei rotational bands based on the ground or isomer states are excited.

The advantages of Coulomb excitation over the investigation of these nuclei in radioactive decay or in nuclear reactions is that in this case only levels associated with $E2$ transitions are occupied, and the γ-ray spectrum is much simpler for analysis and interpretation. This applies especially to odd–odd nuclei, in which the spectrum of the levels and the transitions between them are very complicated.

We listed above reactions with secondary beams that have cross sections 10^{-24}–10^{-26} cm^2. Radioactive beams can also play a decisive role in investigations of reactions with smaller cross sections—complete fusion reactions, many-nucleon transfer reactions, fission. The investigation of each of these reactions makes it possible to obtain very important new information, both about the reaction mechanism and the characteristics of the interacting nuclei. Radioactive beams make it possible to investigate the stability of superheavy nuclei in the region of the closed shells $Z=114$, $N=182$.

Complete fusion reactions with formation of transfermium elements

The observation of resonance structure in the excitation functions of the fusion cross section in the interaction of light nuclei demonstrated the important role of nuclear structure and also of the number of neutrons on the height and shape of the fusion barriers.[63] Subsequently similar results were obtained for heavier nuclei as well, as a result of which it was concluded that there must be some fluctuative barrier that depends on the structure of the interacting nuclei. The possibility of increasing the fusion barrier by several orders of magnitude through excitation of giant resonances in interacting exotic nuclei was demonstrated in Ref. 64. The result

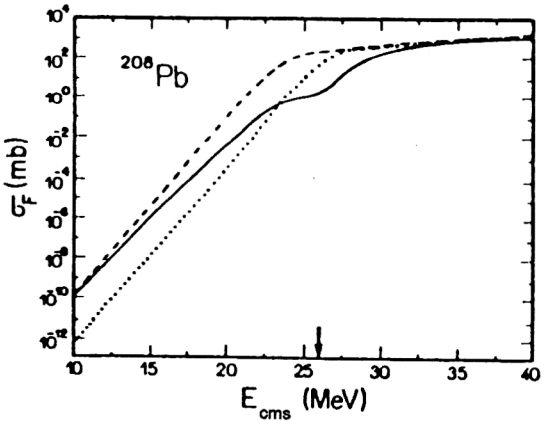

FIG. 37. Theoretical calculations of the excitation function for the ^{11}Li+^{208}Pb complete fusion reaction. The dotted curve gives the calculations without allowance for the soft mode of the resonance, the dashed curve is with allowance for the soft mode, and the solid continuous curve is with allowance for the soft mode and halo dissociation.[64]

of these calculations is shown in Fig. 37 for the ^{11}Li+^{208}Pb system; the dashed line is the calculated value of the cross sections in the case of excitation of resonances in this system. This raising of the cross section and the possibility of deep below-barrier fusion (low excitation energies) can be used to synthesize transfermium nuclei in reactions with radioactive beams.

Synthesis of new transfermium elements, including superheavy elements in the region of $Z=114$ and $N=182$, is one of the most interesting problems of heavy-ion physics. One of the fundamental questions in this problem is the method of producing the superheavy nuclei. This problem is associated, first, with the production of nuclei with maximum number of neutrons, close to $N=184$. Second, it is necessary in the fusion reaction to obtain a compound nucleus with minimum excitation energy in order to ensure that the produced nucleus can, by evaporation of neutrons or charged particles, go over to the ground state, avoiding the fission stage. The first condition can be satisfied only in the presence of radioactive beams. Indeed, one of the optimum reactions for the synthesis of superheavy nuclei induced by

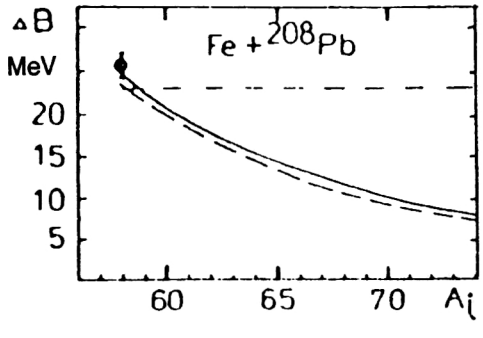

FIG. 38. Dependence of the "extra push" energy (ΔB) on the mass number of the iron isotopes. The dashed and solid continuous curves are obtained under assumptions of different values of the effective fissility parameter (X_{eff}).[64]

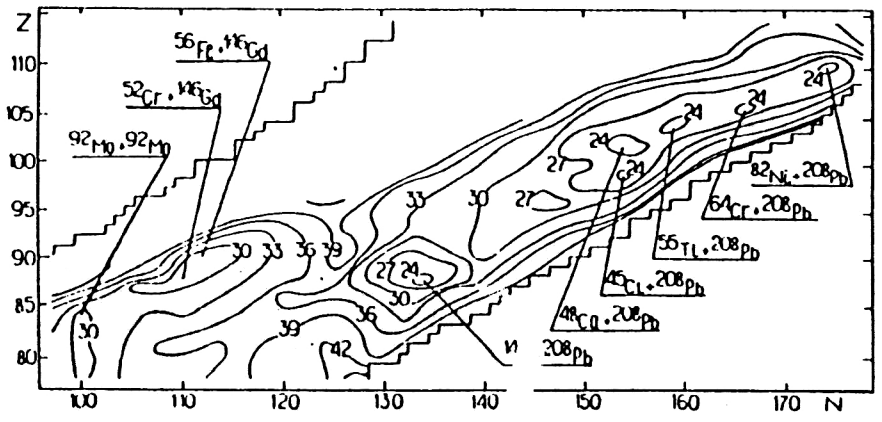

FIG. 39. The $N-Z$ diagram for heavy nuclei with values of the minimum excitation energy for different reactions.

stable nuclei is the $^{248}Cm+^{48}Ca$ reaction; as a result of the evaporation of neutrons and charged particles, it gives nuclei with neutron number much less than 184. Therefore, beams of nuclei such as ^{52}Ca,^{54}Ti ^{64}Fe can give the possibility of synthesizing nuclei near shells with $N=184$. In addition, as has been shown in a number of studies, fusion reactions with exotic nuclei having large radius of the neutron distribution occur with large cross section. Thus, using beams of the radioactive nuclei ^{8-11}Li,$^{10,11}Be$,$^{14-16}C$,$^{16-18}N$,$^{19-22}O$,$^{20-23}F$. $^{23-25}Ne$, and $^{24-31}Na$ with the neutron-rich actinide targets ^{244}Pu, ^{248}Cm, ^{249}Bk, $^{251,252}Cf$, and ^{254}Es it is possible to obtain and study the decay properties of a large number of new neutron-rich nuclei of actinide and transactinide nuclides. It should be noted here that an important factor that reduces the probability of fusion of two heavy nuclei is the "extra push" effect,[65] which increases the minimum energy needed for fusion by an amount ΔB, which can be approximated by the expression[64]

$$\Delta B=\begin{cases}0 & \text{for } x<0.567\\ 189(x_{\text{eff}}-0.567)^2+1.04\cdot 10^5(x_{\text{eff}}-0.567)^6(\text{MeV}) & \text{for } x>0.567,\end{cases} \tag{39}$$

where

$$x_{\text{eff}}=(Z^2/A)_{\text{eff}}/(Z^2/A)_{\text{cr}},$$

$$\left.\begin{array}{c}(Z^2/A_{\text{eff}})=4Z_iZ_t/[A_i^{1/3}A_t^{1/3}(A_i^{1/3}+A_t^{1/3})]\\ (Z^2/A_{\text{cr}})=50.883[1-1.7826((A_{\text{cn}}-2Z_{\text{cn}})/A_{\text{cn}})^2]\end{array}\right),$$

the index i identifies the bombarding ion, and the index t the target.

Figure 38 shows the calculated (in Ref. 64) dependence of the "extra push" on the mass number of the lead isotopes in the $Fe+^{208}Pb$ reaction, which leads to element 108. It can be seen that with increasing mass number of the isotope the value of ΔB decreases. Figure 39 shows the $N-Z$ diagram for heavy compound nuclei with minimum excitation energy for different reactions. It can be seen from the figure that, using the fusion reactions of radioactive beams such as

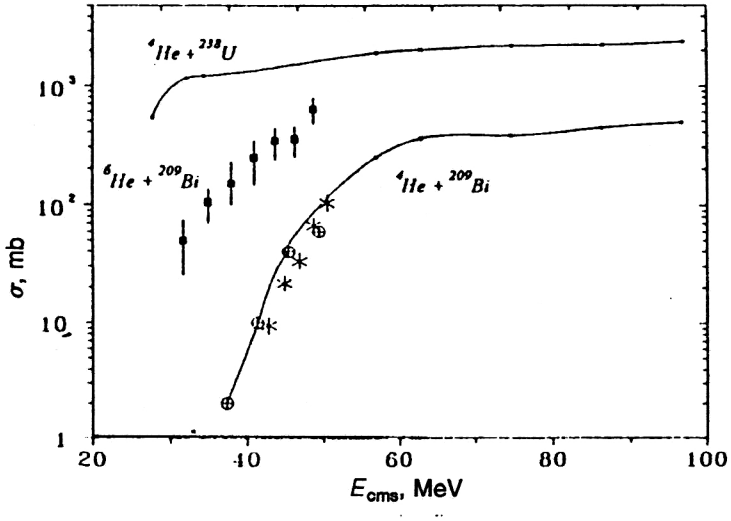

FIG. 40. Dependence of the cross section for fission of ^{209}Bi nuclei on the energy of the bombarding ^{6}He particles (closed symbols) and ^{4}He (open symbols and stars).[66]

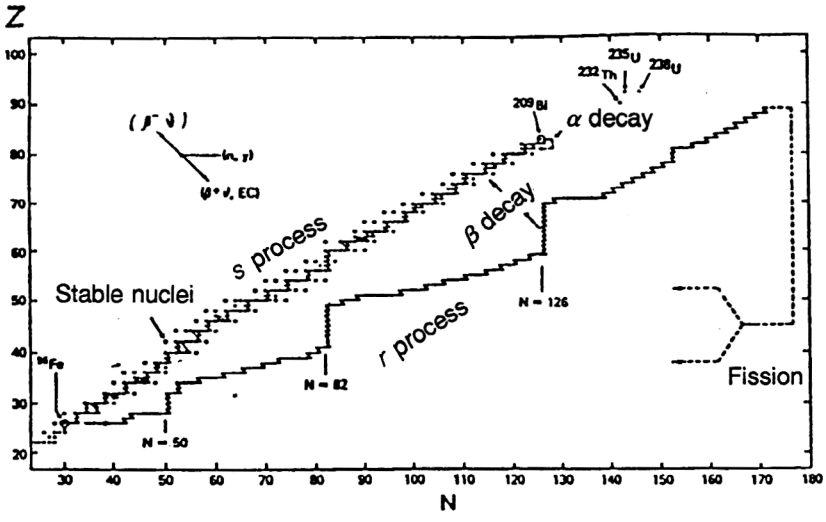

FIG. 41. Neutron capture chains for the s and r processes in the (N,Z) plane. They begin at iron and end at ^{209}Bi (s process) and at heavier elements (r process). The s process ends when the nuclei begin to fission. The chains are calculated for neutron density 10^{24} cm^{-3} and temperature T_9.

^{82}Ni,^{64}Cr,^{56}Ti, and others, it is possible to obtain compound nuclei with $Z=110$, 106, 104, respectively, with minimum excitation energy ~25 MeV. This extremely interesting question requires additional experimental investigation. Such reactions can be used to study exotic fusion modes. In particular, fusion—fission reactions with radioactive beams can be used effectively to study bimodal fission of nuclei in the region of fermium, fission of nuclei from isomer states in the region of masses $A=150$–200, the fission of shape isomers with high spin, etc.

The excitation function of the fission reaction of the compound nucleus ^{215}At produced by the interaction of a radioactive beam of ^{6}He with ^{209}Bi nuclei was studied for the first time in the recent investigation of Ref. 66. The data are given in Fig. 40. It can be seen that the cross section for fission with the ^{6}He nuclei is an order of magnitude higher than with the ^{4}He nuclei and that fission of the ^{215}At nucleus occurs with relatively high probability deeply below the barrier. This result can be explained by the fact that in the case of fusion reactions with neutron-rich nuclei the repulsive potential acts at greater distances than for stable nuclei, and, as a rule, the Coulomb barrier between nuclei with halo can be lower than between stable partners.[64] In addition, excitation of the soft mode of the giant resonance in the excitation of exotic nuclei also greatly facilitates fusion.[64] This first result from the investigation of fission in reactions with radioactive beams shows the new possibilities of studying the fission of such compound nuclei that cannot be obtained in reactions with heavy ions in the case of acceleration of stable isotopes.

Radioactive beams and nuclear astrophysics

The main problems of modern nuclear astrophysics are to model the processes of energy release in the formation and explosion of stars, and also to model the formation of the different elements (nucleosynthesis) in the universe. Both these problems are directly related to investigations by the methods of nuclear physics of, in the first case, the effective cross sections for the interaction reactions of different nuclei, including radioactive nuclei with energies from the Coulomb barrier and below to several hundred MeV/nucleon, and, in the second case, of the masses and lifetimes of nuclei with respect to β decay of the different nuclei.

The main role in an astrophysical processes is played by thermonuclear reactions involving capture of protons, α particles, or neutrons by different nuclei, including unstable ones. Determination of the rate at which such reactions take place is a complicated experimental problem. The cross section also depends strongly on the temperature of the object. In the process of nonexplosive evolution of a star, its temperature is relatively low, and the effective cross section of the reactions is in the range from picobarns to nanobarns. In the explosion of stars, the temperature is very high (10^8–10^9°K), and the effective cross section is millibarns. To model these processes, it is necessary to have a wide range of radioactive nuclei that play the main role in the explosion of stars. In this case, one can use the direct method of investigating the characteristics of reactions with radioactive beams, using for this a target of hydrogen and helium. We give some examples of such reactions. In recent years, astrophysicists have been actively discussing the possibility of the existence of inhomogeneities in the distribution of the hadronic matter after the transition from the quark to the hadronic phase. Under these conditions, the abundance of elements with $A\approx 7$ can be appreciably greater than is predicted by the standard model.[67] For nucleosynthesis in such an inhomogeneous, so-called big-bang process, the most important reactions are those of the type ^{8}Li$(\alpha,n)^{11}$B, ^{6}He$(\alpha,n)^{9}$Be. To model the hot proton–proton channel, which can be present in supernova explosions, it is of interest to measure the rate of reactions such as ^{7}Be$(p,\gamma)^{8}$B, ^{7}Be$(\alpha,\gamma)^{11}$C, ^{8}B$(p,\gamma)^{9}$C, ^{11}C$(p,\gamma)^{12}$N.

The classical CNO cycle in stars takes place when the ^{13}N$(p,\gamma)^{14}$O reaction is more probable than β decay of the ^{13}N nucleus. These processes play an important role in the formation of supernova and supermassive objects. To investigate the CNO cycle, one can also use reactions with radioactive nuclei such as ^{19}Ne$(p,\gamma)^{20}$Na, ^{14}O$(\alpha,p)^{17}$F, ^{15}O$(\alpha,\gamma)^{19}$Ne.

The simple transition from the hot NeNa–MgAl cycle to

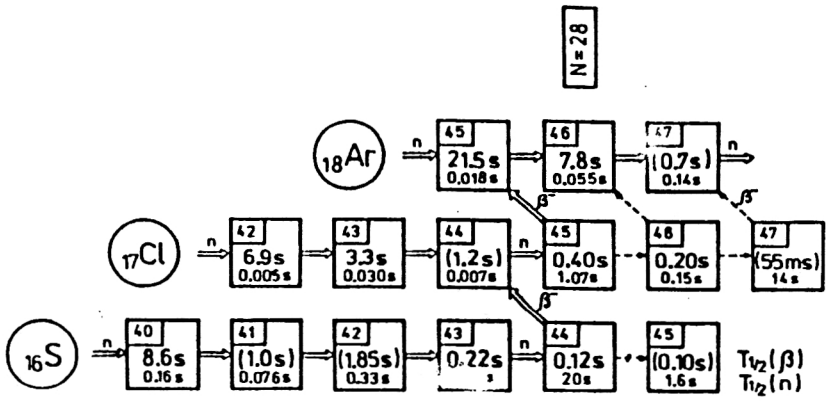

FIG. 42. Neutron capture chains in the $_{16}$S and $_{18}$Ar channels for temperature $8T_8$ and neutron density $s\cdot10^{-5}$ mole·cm^{-3}. The isotopes ^{44}S and ^{45}Cl are turning points for neutron capture. This scheme is obtained as the result of joint Dubna–GANIL–Mainz experiments.[68]

the cold cycle depends on the rates of reactions such as ^{20}Na$(p,\gamma)^{21}$Mg, ^{22}Na$(p,\gamma)^{23}$Al. The experimental determination of the rate of the ^{26m}Al$(p,\gamma)^{27}$Si reaction using beams of radioactive isomer nuclei is a very important experiment in astrophysics.

Some types of CNO and NeNa–MgAl hot cycles can occur in $2p$ and αp processes such as ^{15}O$(\alpha,\gamma)^{19}$Ne and ^{14}O$(\alpha,p)^{17}$F when the probability of these reactions is greater than the probability of β decay of the nuclei ^{15}O and ^{14}O. These processes take place in some type I supernovas. Such situations are readily investigated in the reactions ^{15}O$(\alpha,\gamma)^{19}$Ne, ^{14}O$(\alpha,p)^{17}$F, and also ^{26}Si$(p,\gamma)^{27}P$, ^{31}Si$(p,\gamma)^{32}$Cl, ^{35}Ar$(p,\gamma)^{36}$K, ^{39}Ca$(p,\gamma)^{40}$Sc, ^{43}Ti$(p,\gamma)^{44}$V.

Another indirect way of determining the reaction rates, and also the relative abundance of elements, is to obtain spectroscopic data on the properties of nuclei far from the stability line. These data are used to describe the process of slow capture of neutrons (s process) and rapid capture of neutrons (r process). Figure 41 shows nucleosynthesis paths in the r and s processes. The chains of the s process pass near the stability line, the paths of the r process are almost at the stability boundaries of the neutron-rich nuclei.

We mention the example of an experiment made in the framework of the Dubna–GANIL (France)–Mainz (Germany) collaboration, in which the decay characteristics of neutron-rich S, Cl, and Ar nuclei were measured.[68] Such experiments can be used to obtain fundamental characteristics of astrophysical processes. We present below the probabilities of delayed neutron decay obtained in these experiments and compared with calculated values:

Nuclei	$T_{1/2}$ (exp), ms	P_n (exp), %	$T_{1/2}$ (theor.), ms	P_n (theor.), %
^{44}S	121±10	18.5±5	313	35
^{45}Cl	405±35	24±6.5	1719	25
^{46}Cl	202±50	60±17	180	30
^{47}Cl		<7	200	730

On the basis of the obtained data, a scheme of rapid neutron capture in the region of the S, Cl, and Ar nuclei was constructed (Fig. 42). In accordance with this scheme, the maximum time of irradiation with neutrons was determined, together with the neutron flux and the temperature of the star corresponding to it that emits the neutrons (see Fig. 43). As can be seen from Fig. 41, in the region of the neutron shells $N=50$, 82, and 126 there is a high probability of neutron capture with production of nuclei at the boundaries of neutron stability, for which $\tau_n > \tau_\beta$, and β decay with increase in Z of the following nucleus. These so-called turning points are fundamental in the question of nucleosynthesis. The use of radioactive beams makes it possible to investigate in detail the properties of neutron-rich and neutron-deficient nuclei and thus obtain important information about the processes taking place in the universe.

Applied investigations with beams of radioactive nuclei

Recently, heavy-ion beams have been widely used for investigations in the field of solid-state physics.[69] The prop-

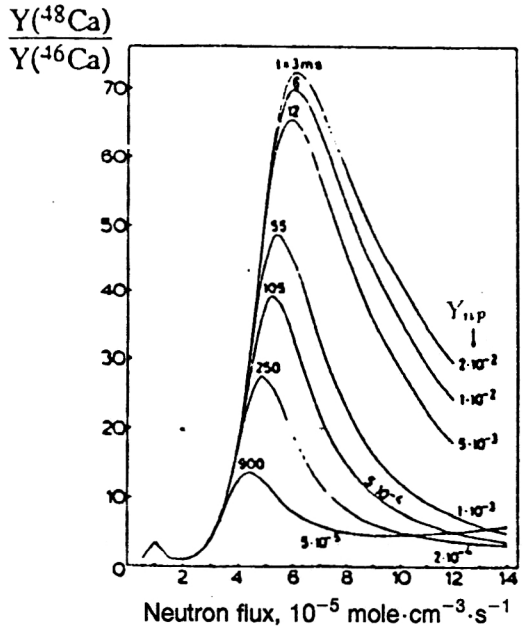

FIG. 43. a) Ratio ^{48}Ca/^{46}Ca of isotopic abundances as function of the neutron fluxes for different combinations of the irradiation time (t) and the neutron density $Y_n\rho$. For ^{44}S, the experimental value 121 ms is taken. b) The ratio ^{48}Ca/^{46}Ca of the isotopic abundances as function of the different values of the neutron decay probability (P_n) of ^{47}Cl. It can be seen that the observed results for the star EK-1-4-1 can be explained only by a small value of P_n.

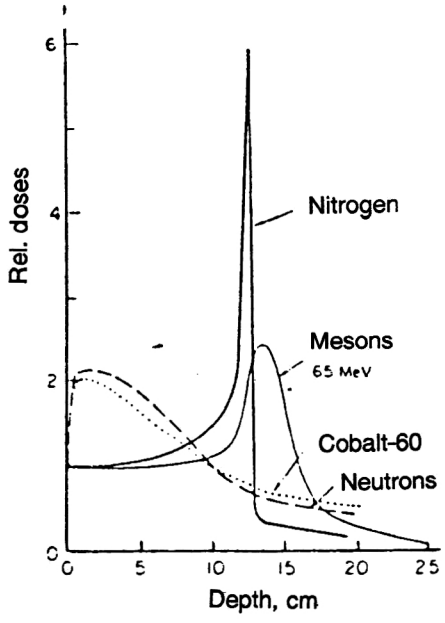

FIG. 44. Relative dose of the distribution of different beams with respect to the depth.

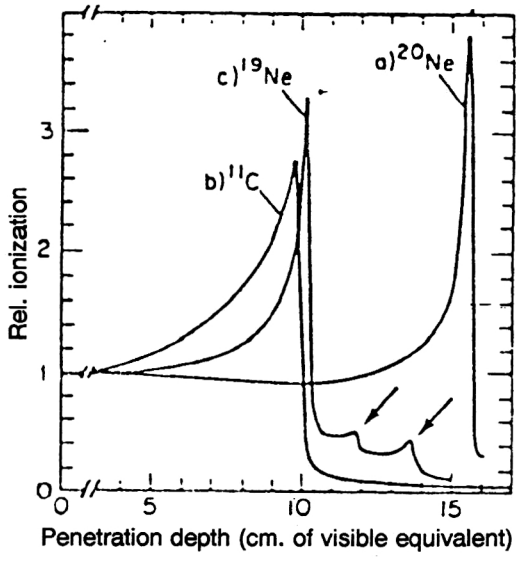

FIG. 45. Bragg ionization curves for the isotopes ^{19,20}Ne,^{11}C.

erties of these beams—the high specific ionization, the strong dependence of the ion range on the charge and mass of the absorbing medium, and the well-defined Bragg absorption curve—make them a unique instrument for investigations at the atomic level. The study of surfaces, the structure of solids (clustering), semiconducting materials, and organic and biological objects—all these problems can be solved using beams of radioactive nuclei. Since at the present time proposals for the use of radioactive beams are only under discussion, it is possible to give only some examples of their possible use.

The channeling effect in crystalline materials can be used to study their structure and composition. Implanting radioactive nuclei in an investigated material and studying its emission (e^+,e^-,α) in different directions, one can determine with high accuracy the position of the crystallographic axes, and also the presence and position of impurities. Migration of impurities as a function of the temperature is a subject of great interest. Implanting radioactive nuclei at low temperatures, and then heating the sample and measuring the radiation yields at different angles, it is possible to obtain information about the change in the structure of the material and the contained impurities as function of the temperature.

Mössbauer spectrometry with radioactive nuclei opens up great possibilities for investigating the structure of solids. Analysis of the Mössbauer spectrum (isomer shift, change in the quadrupole and magnetic moments) gives information about the density of electrons and the gradients of the electric and magnetic fields in which the implanted radioactive nucleus is situated. In this case, the amplitude of resonant absorption is determined by the mean vibration amplitude of the nuclear probe. The Doppler effect can also change the velocity of the nuclear probe as a function of the position of its diffusion, and in principle this can also be used to study the local structure of the material. In addition, there is also a proposal to use the method of perturbed angular correlations in hyperfine interactions. Measuring the angular correlations of the emission of the nuclear probe, one can obtain information about the properties of the hyperfine magnetic fields, and also about the gradient of the electric field around the nuclear probe.

Also promising is the use of radioactive beams to study various organic media and biological objects.[70] Figure 44 shows the dependence of the relative irradiation dose of a biological object with respect to the depth for different sources. It can be seen that only heavy ions give a narrow distribution with weak irradiation dose before and after the Bragg maximum. This demonstrates the high efficiency of the use of heavy ions, for example, for radiotherapy. This possibility is illustrated by Fig. 45, which gives the Bragg ionization curves for beams of ^{20}Ne (425 MeV/A) and ^{19}Ne obtained by fragmentation of this beam, and also ^{11}C obtained by fragmentation of a ^{12}C (240 MeV/A) beam.[70] It can be seen that for the different isotopes the Bragg maximum differs significantly. These qualities of radioactive beams can be used not only for their direct local action on definite biological objects but also, by implanting a radioactive nucleus at a rigorously fixed position, one can influence the objects by means of the emission of the radioactive nuclide. This extremely important direction in the use of radioactive beams may have a great future in genetics, radiobiology, and radiotherapy.

I am deeply grateful to Professor Yu. Ts. Oganesyan, Yu. P. Gangrskiĭ, G. M. Ter-Akop'yan, A. A. Oglobdin, and F. A. Gareev for fruitful discussions and ideas on the subject of this review. I also thank K. Detraz, A. Müller, W. Mittig, B. Sherill, and T. Kobayashi for helpful advice and comments. I am grateful to R. Kalpakchieva and Z. D. Pokrovskaya for assistance in preparing the review.

[1] G. N. Flerov, Peaceful Uses of Atomic Energy, Vol. 7 (Int. Atomic Energy Agency, Vienna, 1972), p. 471.
[2] V. A. Karnaukhov and G. M. Ter-Akop'yan, Yad. Fiz. **1**, 61 (1965) [Sov. J. Nucl. Phys. **1**, 41 (1965)].

[3] V. I. Goldanski, Nucl. Phys. **27**, 648 (1961).
[4] S. M. Polikanov *et al.*, Zh. Eksp. Teor. Fiz. **42**, 1464 (1962) [Sov. Phys. JETP **15**, 1016 (1962)].
[5] V. M. Strutinsky, Nucl. Phys. **A95**, 420 (1967).
[6] G. F. Gridnev, V. V. Volkov *et al.*, Nucl. Phys. **A142**, 385 (1970).
[7] Yu. Ts. Oganesyan *et al.*, Yad. Fiz. **6**, 306 (1967) [Sov. J. Nucl. Phys. **6**, 222 (1968)].
[8] Yu. Ts. Oganessian, *in Classical and Quantum Mechanical Aspects in Heavy Ion Collisions. Lecture Notes in Physics*, Vol. 33 (Heidelberg, 1975), p. 221.
[9] Yu. É. Penionzhkevich *et al.*, Fiz. Elem. Chastits At. Yadra **17**, 165 (1986) [Sov. J. Part. Nucl. **17**, 65 (1986)].
[10] C. Detraz and D. J. Vieira, Ann. Rev. Nucl. Part. Sci. **39**, 407 (1989).
[11] J. L. Belmont, in *Proc. of the Intern. Conf. on Exotic Nuclei, Foros*, edited by Yu. Penionzhkevich and R. Kalpakchieva (World Scientific, Singapore, 1991), p. 321.
[12] V. Borrel *et al.* Z. Phys. A **314**, 191 (1983).
[13] A. S. Goldhaber, Phys. Lett. **53B**, 366 (1974).
[14] Y. Blumenfeld *et al.*, Nucl. Phys. **A455**, 357 (1986).
[15] R. Anne *et al.*, Nucl. Instrum. Methods **A257**, 215 (1987).
[16] G. Rudstam, Z. Naturforsch. **21K**, 1027 (1966).
[17] Silberg and C. H. Tsao, Astrophys. J. Suppl. **25**, 315 (1973).
[18] K. Suemmerer, in *Proc. of the Intern. Workshop on Phys. and Techn. of RNB*, edited by J. F. Bruandet *et al.* (Dourdan, 1992), p. 273.
[19] M. Huyse and P. V. Duppen, in Proc. of the *Sixth Intern. Conf. on Nuclei Far from Stability*, edited by R. Neugart and A. Woehr (Bernkastel-Kues, 1992), p. 887.
[20] H. L. Ravn, in ISOLDE User's Guide, edited by U. J. Kluge (CERN, 86-05, 1986).
[21] H. Doubre, Preprint GANIL P92-28 (1992); H. Doubre *et al.*, Preprint GANIL R93-11 (1993).
[22] H. L. Ravn *et al.*, in *Proc of the Sixth Intern. Conf. on Nuclei Far from Stability*, edited by R. Neugart and A. Woehr (Bernkastel-Kues, 1992), p. 919.
[23] D. K. Olsen *et al.*, in *Proc. of the 13th Intern. Conf. on Cyclotrons and Their Application*, edited by E. Dutto and M. K. Craddock (Vancouver, 1992), p. 741.
[24] W. Mittig *et al.*, Preprint GANIL 93-04 (1993).
[25] R. E. Pollock, Ann. Rev. Nucl. Part. Sci. **41**, 357 (1991).
[26] H. Emling, Nucl. Phys. **A250**, 687 (1990).
[27] O. N. Malyshev *et al.*, Preprint R9-92-15 [in Russian], JINR, Dubna (1992).
[28] Yu. Ts. Oganessian, Yu. E. Penionzhkevich, and G. M. Ter-Akopian, in *Proc. of the Intern. Symposium Structure and Reactions of Unstable Nuclei*, Niigata, 1992, edited by E. K. Ikeda and Y. Suzuki (World Scientific, Singapore, 1991), p. 300.
[29] Yu. Ts. Oganessian *et al.*, Z. Phys. A **341**, 217 (1992).
[30] D. H. Wilkinson, Phys. Lett. **11**, 243 (1964).
[31] G. T. Garvey and I. Kelson, Phys. Rev. Lett. **16**, 197 (1966).
[32] A. T. Migdal, Yad. Fiz. **16**, 427 (1972) [Sov. J. Nucl. Phys. **16**, 238 (1973)].
[33] A. S. Jensen *et al.*, Nucl. Phys. **A431**, 393 (1984).
[34] A. A. Ogloblin and Yu. E. Penionzhkevich, in *Treatise on Heavy Ion Science*, Vol. 8 (Plenum Press, New York, 1989), p. 261.
[35] Yu. S. Lutostansky *et al.*, in *Proc. of the Fifth Intern. Conf. on Nuclei Far from Stability* (Ontario, 1987), p. 727.
[36] D. Guillemaud-Mueller, Yu. E. Penionzhkevich *et al.*, Phys. Rev. C **41**, 937 (1990).
[37] N. A. Ott, Yu. E. Penionzhkevich *et al.*, Preprint E7-91-149, JINR, Dubna (1991).
[38] J. M. Bang *et al.*, in *Proc. of the Sixth Intern. Conf. on Nuclei Far from Stability*, edited by R. Neugart and A. Woehr (Bernkastel-Kues, 1992), p. 299.
[39] I. Tanihata *et al.*, Phys. Rev. Lett. **55**, 2676 (1985).
[40] A. C. C. Villari, Yu. E. Penionzhkevich *et al.*, Phys. Lett. **268B**, 345 (1991).
[41] T. Minamisono *et al.*, Phys. Rev. Lett. **69**, 2058 (1992).
[42] T. Kobayshi, in *Proc. of the Fourth Intern. Conf. on Nucleus-Nucleus Collisions* (Kanazawa, 1991); Preprint RIKEN-AF-NP-104.
[43] Yu. É. Penionzhkevich, in *Proceedings of the International Seminar School on Heavy-Ion Physics*, edited by Yu. P. Oganesyan, Yu. É. Penionzhkevich, and R. Kalpakchieva, Vol. 1 [in Russian] (Dubna, 1993), p. 42.
[44] E. Y. Berlovich, in *Proc. of the Intern. Conf. on Nuclei Far from Stability*, Leysin (CERN Report 70–30, 1970), p. 497.
[45] M. Langevin *et al.*, Phys. Lett. **146B**, 176 (1984).
[46] Yu. S. Lyutostanskiĭ, Izv. Akad. Nauk SSSR, Ser. Fiz. **50**, 835 (1986).
[47] J. P. Dufour *et al.*, in Proc. of the Third Intern. Conf. on Nucleus–Nucleus Collisions (St Malo, 1988), p. 26.
[48] B. M. Sherill *et al.*, in *Proc. of the Sixth Intern. Conf. on Nuclei Far from Stability*, edited by R. Neugart and A. Woehr (Bernkastel-Kues, 1992), p. 891.
[49] K. Ogawa, in *Proc. of the Intern. Conf. AMCO7*, edited by O. Klepper (Darmstadt-Secheim, 1984), p. 530.
[50] Yu. Ts. Oganessian, Yu. E. Penionzhkevich *et al.*, Nucl. Phys. **A303**, 259 (1978).
[51] R. J. Smith *et al.*, Phys. Rev. C **43**, 761 (1991).
[52] Yu. E. Penionzhkevich *et al.*, Z. Phys. A **341**, 315 (1992).
[53] N. K. Skobelev *et al.*, Izv. Akad. Nauk SSSR, Ser. Fiz. **55**, 2203 (1991).
[54] M. Lewitowicz *et al.*, in *Proc. of the Sixth Intern. Conf. on Nuclei Far from Stability*, edited by R. Neugart and A. Woehr (Bernkastel-Kues, 1992), p. 337.
[55] A. S. Dem'yanova *et al.*, Nucl. Phys. **A553**, 727 (1993).
[56] A. S. Dem'yanova *et al.*, in *Proceedings of the International Seminar School on Heavy-Ion Physics*, D7-90-42 (JINR, Dubna, 1990), p. 480.
[57] Y. Knoll and R. Schaeffer, Ann. Phys. (N.Y.) **97**, 307 (1976).
[58] M. Mermaz *et al.*, Phys. Rev. C **34**, 1988 (1986).
[59] E. Stiliaris *et al.*, Phys. Lett. **223B**, 291 (1989).
[60] H. G. Bohlen *et al.*, Phys. Lett. **37B**, 451 (1971).
[61] I. Tanihata, in *Proc. of the Intern. School-Seminar on Heavy Ion Physics*, Vol. 1, edited by Yu. Ts. Oganessian, Yu. E. Penionzhkevich, and R. Kalpakchieva (Dubna, 1993), p. 3.
[62] Yu. A. Budagov *et al.*, Preprint R13-88-927 [in Russian], JINR, Dubna (1988).
[63] S. G. Steadman *et al.*, Ann. Rev. Nucl. Sci. **36**, 649 (1986).
[64] M. S. Hussein *et al.*, Nucl. Phys. **A531**, 191 (1991).
[65] A. S. Iljinov *et al.*, in *Proc. of the First Intern. Conf. on RNB, Berkeley*, edited by W. D. Myers, J. M. Nitschke, and E. B. Norman (World Scientific, Singapore, 1989), p. 289.
[66] N. K. Skobelev, Yu. E. Penionzhkevich *et al.*, JINR Rapid Commun. No. 4(61) (Dubna, 1993), p. 36.
[67] C.-A. Barnes *et al.*, in *Research Reports in Physics: Nuclear Astrophysics*, edited by M. Lozano, M. I. Gallaraldo, and J. M. Arias (Springer-Verlag, Berlin, 1988).
[68] K. L. Kratz *et al.*, Preprint IPNO DRE 91-14, Orsay (1991).
[69] H. Haas, in *Proc. of the Workshop on the Production and Use of Intense RNB* (Oak Ridge, 1992); Preprint ORNL Conf.-9210121, p. 83.
[70] R. Bimbot, in *Proc. of the Second Intern. Conf. on RNB*, edited by Th. Delbar (Louvain-la-Neuve, Belgium).
[71] European Radioactive Beam Facilities. NuPECC Report by Study Group, May (1993).

Translated by Julian B. Barbour